Chapter 10
Surface Engineering of Graphene-Based Polymeric Composites for Energy Storage Devices

Debajani Tripathy, Ankita Subhrasmita Gadtya, Bibhuti B. Sahu, and Srikanta Moharana

Abstract Graphene is a promising nanocarbon material with exceptional features such as a large surface area and outstanding electrical and thermal properties. It has the potential to be a new creation of reinforcing material for polymer composites owing to its low mass density, large specific surface area, excellent compatibility, the inexpensive cost to create compared to carbon nanotubes, and attractive flexibility. The several approaches for synthesizing graphene and distributing it in polymer matrices are explored. This chapter focuses on a summary of the surface alternation of graphene with various synthetic techniques and the preparation and properties of graphene-based different polymer nanocomposites. This chapter provides a broad overview of the nanocomposite synthesis, properties, and finally prospective application of polymer-graphene nanocomposites in various energy storage sectors.

Keywords Graphene · Graphene surface alternation · Polymer composites · Energy storage

10.1 Introduction

Nanoscience is a new field that is growing very quickly right now. It can be beneficial to several different sectors, including computing, sensors, biology, and technology, among others. Nanoparticles of different sizes, shapes, and properties have been found, which has led to a lot of interesting progress in this field. Researchers have found that nanoscale fillers in polymer nanocomposite composites make them

D. Tripathy · A. S. Gadtya · S. Moharana (✉)
Department of Chemistry, School of Applied Sciences, Centurion University of Technology and Management, R.Sitapur, Paralakhemundi, Odisha 761211, India
e-mail: srikantanit@gmail.com; srikanta.moharana@cutm.ac.in

B. B. Sahu
Basic Science and Humanities Department, Nalanda Institute of Technology (NIT), Bhubaneswar, Odisha 751024, India

S. Moharana et al. (eds.), *Emerging Nanodielectric Materials for Energy Storage*, Nanostructure Science and Technology, https://doi.org/10.1007/978-3-031-40938-7_10

better at mechanical, electrical, thermal, and optical performances [1–3]. There are various types of multifunctional nanocomposite materials are made with the use of nanofillers like carbon nanotubes, nano-clay, graphene, and metal or ceramic nanoparticles. Recent years have seen extensive research into conductive nanofillers-reinforced polymer composites due to their exceptional multifunctional capabilities when compared to those of traditional conductive polymer composites [4–7]. However, with the incorporation of electrically conductive nanoparticles into non-conducting polymers, electron conduction is obtained [8]. Antistatic materials, electromagnetic interference (EMI) shielding, sensors, and conductors are just a few of the many uses for conducting polymer composites, which are advantageous over intrinsic conducting polymers due to their ease of production, cost-effectiveness, and adaptability in electrical characteristics. Because of the low filler levels possible with these conductive fillers, the composites either keep or improve the electrical and mechanical recital of the matrix. Thus, the composite system with nanomaterial reinforcements ought to have enhanced thermal conductivity [9–11]. The various carbon-based allotropes including carbon nanotubes (CNTs) and graphene-based materials are used to generate superior-performing electrically directing composites [12]. These composites are among the most promising nanofiller materials owing to their outstanding mechanical and thermal capabilities, remarkable chemical inertness, and the ability to have their electrical properties modified [13]. There are different parameters including complex processing, poor surface chemistry control, weak interfacial contact with the polymeric matrix, and agglomeration are some of the CNT's drawbacks [14]. The high cost of producing carbon nanotubes (CNTs) is another issue with their use as nanofillers [15]. Thus, it is difficult to mass-produce useful composite materials based on CNTs. When carbon fibers will not cut it and nanotubes are out of reach due to cost, where does a frugal materials scientist turn for a workable conductive composite? [16]. Graphene is the name of the material in the issue, and it exists exclusively in a two-dimensional form. Graphene-based materials have recently emerged as a viable choice for application in state-of-the-art high-performance nanocomposites [12].

The growing number of research papers on graphene shows that academics and businesses are becoming more interested in this material. Over the past few times, the number of graphene patents has steadily grown. These patents have been filed for a wide range of uses, such as characterization, polymer composites, transparent displays, transistors, capacitors, solar cells, biosensors, conductive inks, windows, saturable absorbers, and photodetectors [17]. The total number of newly found fullerenes climbed substantially over the decade from 2005 to 2014. Yet, graphene is the most recently formed nanocarbon and also shows the greatest rate of growth. Although just a few hundred papers were published on graphene in its first three years, interest in the material grew rapidly. Graphene studies have increased rapidly in popularity. As compared to articles on carbon nanotubes (CNTs), those on graphene were on par in 2013, but in 2014, they substantially exceeded their CNT counterparts. In terms of where nanocarbon research has been published, the United States and China stand out as the most prolific authors, responsible for well over half of all such studies. This is especially true when it comes to the two hottest nanomaterials of

the moment, carbon nanotubes (CNTs), and graphene [18]. Significant progress in the investigation of graphene polymer nanocomposites is being driven by the revolutionary improvement in polymer properties, such as mechanical, electrical, and thermal conductivity, and chemical, optical, and gas impermeability at a low-level concentration of filler [19]. There are numerous excellent studies based on unaltered graphene-reinforced polymer nanocomposites available. Moreover, surface functionalization plays an important impact in the enhancement of the electrical and mechanical characteristics of the polymer nanocomposite. This typical chapter focuses on graphene and its properties, as well as its production process. The methods utilized to covalently and non-covalently change surfaces are analyzed in depth and brought up to date in this work. We conclude with a discussion of the varied electronic uses for graphene-based polymer nanocomposites and the consequence that surface functionalization has on the electrical conductivity of these materials.

10.2 Graphene-Based Two-Dimensional Nanostructured Materials

Graphene is a two-dimensional carbon allotrope with a thickness of just one atom. It is composed of a honeycomb arrangement of hexagonal crystalline structure with sp^2 carbon atoms in a conjugated system. Although graphene was theoretically conceived in the 1940s, it lacked the thermodynamic stability required for reliable operation in everyday environments [20–22]. In a 2004 tabletop experiment [21], Geim and colleagues at Manchester University successfully distinguished individual graphene layers. The thinnest known substance has been discovered thanks to this groundbreaking discovery, which has opened up new avenues of investigation in the domains of physics, chemistry, biology, and materials science [22, 23]. Graphene has a low coefficient of thermal expansion (CTE), thermal conductivity, young's modulus (1 TPa), and superior optical transmittance along with other desirable characteristics [20]. This graphene-based material shows more perspective than other nanostructured carbon allotropes, like 0D fullerenes and 1D nanotubes.

10.2.1 Preparation of Graphene-Based Materials

There are two different techniques for synthesizing graphene: either from the top-down (a) or from the bottom-up (b) approach. Top-down methods that aim to lessen the van der Waals contacts between graphene layers include mechanical (Scotch tape), chemical (solution-based exfoliation, graphite oxide exfoliation or reduction), and electrochemical (oxidation or reduction and exfoliation) (as shown in Fig. 10.1) [24]. On the other hand, graphene is made via bottom-up techniques, which entail the assembly of minuscule molecular building blocks into sole or many-layered graphene

assemblies through catalytic (e.g., CVD), thermal (e.g., SiC breakdown), or chemical (e.g., organic synthesizing) processes [25]. Graphene is a 2D carbon allotrope, where every single carbon atom connects with every other carbon atom via sp^2. Carbon atoms arrange themselves in honeycomb crystal symmetry, with a bond length of just 0.141 nm. A typical density of graphene is 0.77 g/cm^3. Graphene's surface area per unit mass is thought to be around 2600 m^2/gm^2 [20, 26]. Graphene has amazing electrical, thermal, mechanical, electronic, and optical characteristics, making it the most appealing nanomaterial today. However, it is the reediest and toughest composite ever examined. Tensile strength tests have shown that graphene is comparable to or even exceeds that of carbon nanotubes (CNT), and significantly exceeds that of steel, Kevlar, and additional polymers [27]. To determine the modulus of elasticity of single-layered graphene sheets created by chemically reducing graphene oxide, academic and industrial researchers used the tip of an atomic force microscope to make a small indentation in the core of a modified sheet of graphene. Moreover, an elastic modulus (1TPa) and an inherent strength (130 GPa) have also been calculated for a defect-free monolayer graphene sheet [28, 29]. However, the thermal conductivity of graphene [5000 W/(m^{3}K)] by its electrical conductivity is close to 6000 S/cm [30, 31]. Due to its semi-metallic nature, graphene exhibits several fascinating electrical characteristics. The extraordinary thermodynamic and electrical conductivity of graphene is owing to its exceptionally elevated charge carrier mobility (10 cm^{2}V s^{-1}) [32]. The edge states and any adsorbed or intercalated species have a significant impact on graphene's magnetic properties [33, 34].

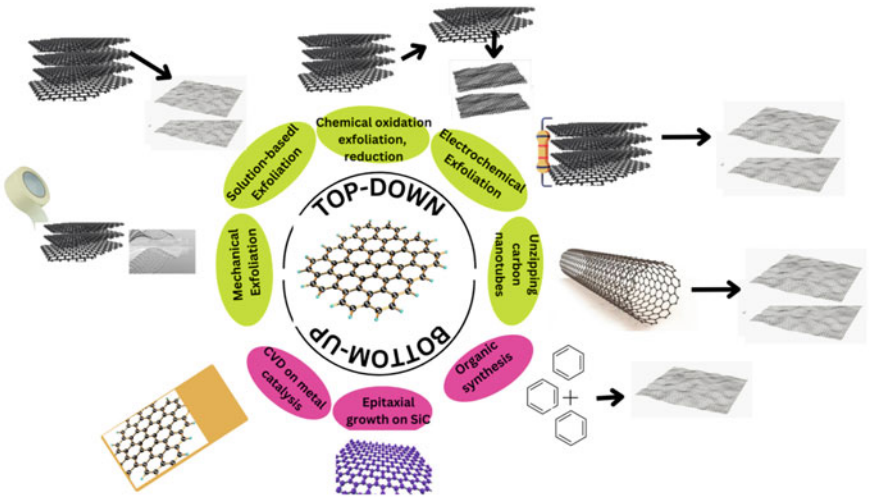

Fig. 10.1 Schematic illustration for preparation of materials based on graphene

10.2.2 Surface Alternation of Graphene

Graphene-based materials tend to stick together more in a polymer matrix, which makes them less friendly to large molecules like polymeric chains [35]. To modify their physiochemical characteristics, graphene and its derivatives are often chemically functionalized. The potential benefits of graphene sheets are immense, but only if the material can be made operational and widely disseminated. Covalent functionalization involves the formation of chemical bonds, while non-covalent functionalization relies only on van der Waals forces.

(a) **Covalent Functionalization**

Covalent superficial alteration of graphene causes hybridization of one or additional sp^2 carbon atoms of the aromatic edifice, leading to forfeiture of electronic conjugation and a strain in the plane. As the hybridization has changed, the carbon atoms (sp^2hybridized) which are ordinarily in a flat plane must now adopt the sp^3 tetrahedral geometry. Specifically, this is because carbon atoms at the edge of a molecule are more likely to undergo covalent addition processes [36]. Graphene's dispersibility in organic solvents and water can be improved by covalent organic functionalization, and its characteristics can be combined with those of extra-functional materials like chromophores or polymers [37]. Functionalization can transpire on the interface, the boundaries, and the defects of materials. The chemical techniques used to create graphene are not without problems, including damage to the carbon lattice, structural errors, and the random adsorption of solvent molecules [38, 39]. There are various classes of covalent functionalization have been reported in recent times, which include free radical adding, atomic radical addition, nucleophilic addition, cycloaddition, and electrophilic substitution.

(i) **Cycloaddition Reactions**

In cycloaddition reactions, bond breaking and bond creating occur simultaneously deprived of the creation of anions or cations as intermediates, resulting in a cyclical motion of electrons. The graphene molecule has undergone cycloadditions [2 + 1], [2 + 2], [3 + 2], and [4 + 2]. The most well-known kind of cycloaddition is the 1,3-dipolar and [3 + 2] cycloaddition reaction [40, 41]. Other cycloaddition reactions including (i) [2 + 1] cycloaddition similar to the Bingel reaction, interactions with nitrenes and leading to the creation of cyclopropane or aziridine adducts [42], (ii) [2 + 2] cycloaddition with an aryne or benzyne [43] and (iii) [4 + 2] cycloaddition are two ways to create a cycle with four carbon atoms. An electron-rich diene and an electron-poor dienophile can undergo a cycloaddition via the Diels–Alder mechanism (electron-deficient species) [44]. Graphene has a wide variety of potential uses owing to its capability of functioning as either the diene or dienophile in the Diels–Alder process. Graphene has the potential to induce unanticipated consequences, and it is notoriously difficult to regulate surface modifications. Nitrides and carbenes, in particular, are capable of reacting with solvents as well as one another [45].

(ii) **Free radical Reactions**

Covalent bonds are formed between the aromatic structure of graphene and free radicals, which are extremely reactive organic molecules. These modifications have been accomplished through thermodynamic or photochemical processes. Though, by using superior-energy reactants, unwanted side reactions or lack of homogeneity might occur in the functionalization reaction [46]. The use of aryl diazonium salts in radical addition reactions is widespread. Peroxide addition, Bergman cyclization [47], and Kolbe electro-synthesis [48] are a few such processes. The reactivity of aryl diazonium salts is the subject of this subsection. Tour and his co-workers [49] suggested first successfully putting aryl diazonium salts into graphene. In this step, nitrogen removal, the aryl diazonium ion transforms into an aryl radical. It is hypothesized that the radical aryl moiety contributes an electron to the sp^2-hybridized graphene [50]. This process, however, can generate organic radicals that are not only capable of covalently reacting with graphene but also of self-polymerizing [51]. The amount of graphene sheets has a significant impact on this reaction. Moreover, the bi or multilayer graphene, the reactivity of a solitary graphene slip is found to be 10 times higher, as reported by Strano and his co-workers [52].

(iii) **Nucleophilic Reactions**

Graphene is the material of choice when it comes to making a nucleophilic addition that accepts electrons. The chemical reaction between graphene and poly-9,9′-dihexyfluorene carbazole Nitrogen anions are created on carbazole when it is subjected to the action of a base, which results in the formation of the anionic moiety. Once the two substances react with one another, a covalent connection is created between the nitrogen anion and the surface of the graphene [53, 54].

(iv) **Reaction with atomic Radii**

By using hydrogen, fluorine, and oxygen from the periodic table instead of organic free radicals, the number of unwanted byproducts is kept to a minimum. As a result, the functionalized graphene becomes even as well as consistent. Hydrogenation makes it facile to procedure the secondary C-H bonding because it changes the shape of the lattice when the first hydrogen atom is added. Graphene in its fully hydrogenated form is known as graphene. Graphene can be hydrogenated when subjected to hydrogen-based plasmas [54]. When you fluorinate graphene, you make a single bond between fluorine and carbon, which is similar to hydrogenation but much stronger. There is a lot of functionalization after fluorination, much like there is after hydrogenation [55]. It has been hypothesized that fluorographene will act as an insulator. Typically, one of three techniques is used: The three methods for exfoliating bulk graphite fluoride are: (i) by exposing it to XeF_2 [56], (ii) by etching it with a fluorinated reagent [57], and (iii) by using a liquid phase.

(v) **Electrophilic Reactions**

Graphene's abundance of free electrons makes it amenable to this class of processes. The Friedel–Crafts acylation [58] and the hydrogen–lithium exchange are two types

of substitution processes. Metal-functionalized aromatics are more reactive than their simpler counterparts. Before the hydrogen–lithium exchange, BuLi deprotonates and carbometallizes graphene. An electrophile then interacts with the lithium graphene derivative. The lithium graphene derivative undergoes an instantaneous reaction upon electrophile addition, leading to the conception of covalent bonding [59].

(b) **Noncovalent functionalization**

Non-covalent interactions, such as hydrophobic, van der Waals, and electrostatic interactions, can cause molecules to stick to the surface of graphene [60]. This method of functionalization is noteworthy because it allows molecules to be immobilized straightforwardly and reversibly without disrupting the electrical network [61]. Functionalized non-covalent is essential for the immobilization of proteins, enzymes, medicines, and DNA, particularly in the background of devices, because even a small change in the electrical properties of the system could result in an entire alteration in the structure and characteristics of the system [62, 63]. There has been extensive research into complexes based on graphene, including interactions between non-polar gases and H^+, cations, and anions. Three parts are responsible for its attractive strength: electrostatic, dispersive, and inductive interactions. To make sodium cholate, cetyltrimethylammonium bromide, polyvinylpyrrolidone, triphenylene, and pyrene derivatives are only some of the surfactants that may be employed in an exfoliation approach to creating functionalized graphene from graphite without the use of covalent bonds [64]. On the other hand, along with the single-layer variety, a sizeable amount of few-layered graphene or scattered graphite is likewise produced. Coronene carboxylate produces layers around 100 nm thick [65, 66]. For instance, Bai and his co-workers have developed larger graphene flakes that can be manufactured using perylene derivatives [67, 68].

10.3 Synthesis Process of Graphene-Based Polymer Composites

Graphene-based materials have high strength and high electrical and thermal conductivity making them a potential contender for usage in an extensive range of commercial products, like polymer composites, conductive coatings, fuel cell batteries, and ultra-capacitors. Chemical vapor deposition (CVD), exfoliation, liquid-phase exfoliation, etc., are all examples of top-down ways to make graphene, which can be further divided into bottom-up ways. Owing to their outstanding material characteristics, including yield métier, robustness, electrical and thermal conductivity, and optical properties, polymer nanocomposites (PNC) research has advanced greatly over the last decade, and their applications have grown substantially as a result [69–73]. Graphene possesses excellent dimensional stability, high thermal stability, high gas impermeability, elevated strength and elastic modulus, and high electrical and thermal conductivity [72]. Adding graphene to polymers at a tiny volume percentage may dramatically enhance their characteristics. Furthermore, graphene may be employed

at a lower volume percentage since it has a better surface-to-volume ratio than carbon nanotubes [73]. It may enhance a wide variety of polymer matrix characteristics. As an example, graphene-based nanocomposites are in high demand for use in photovoltaic devices like solar cells because of their low resistivity and high carrier mobility, and because (i) used in lithium-ion batteries (LIBs) such as power density, energy density, and speed of charging in hydrogen fuel cells, (ii) they are used in thermoelectric materials, (iii) used in photovoltaic devices including solar cells owing to their low resistivity and high carrier mobility, and (iv) used as an electrode to raise the electro-catalytic performances [71].

One definition of nanocomposite is a material, which is having any one dimension in the nanoscale. It has made strides in the areas of light, electricity, and magnetism and has desirable features like thermal stability and mechanical strength. Polymer, metal, or ceramic matrices are used to create nanocomposites, which are then filled with nanoparticles (graphene, nanotubes, and clays) [74]. The material's mechanical, thermal, and electrical characteristics are all improved by adding fillers. Polymeric nanocomposites are the most adaptable of all nanomaterials, finding use in several fields such as energy, electronics, health care, and more [71, 72]. Micro-composites, intercalated nanocomposites, and exfoliated nanocomposites are the three main categories of polymer composites based on the distribution of nanosized layers. In the micro-composites' structure, the graphene sheets are disseminated as particles inside the polymer matrix, yet the graphene platelets themselves are unharmed [75]. When distinct polymer chains are inserted between graphene layers, this creates an introduced structure. The exfoliated amalgams' graphene films are evenly distributed throughout the polymer backbone. Since exfoliation maximizes the surface area of contact between the polymer and the filler, it is the preferred morphology for nanocomposites. This leads to improved bonding and superior mechanical characteristics [76]. Graphene nanocomposites' characteristics are affected by a number of factors, including the filler's chemical compatibility with the matrix, the filler's volume fraction, and processing conditions, including dispersion and exfoliation. For optimal performance, it is necessary to use suitable manufacturing techniques. Additionally, the recital eminence of nanomaterials is closely correlated with the rate of dispersity. In-situ polymerization, melt intercalation, and exfoliation adsorption are the three main ways to create polymer nanocomposites [75–77].

Heat or radiation can be used to start polymerization in place by mixing adapted graphene through a monomer or pre-polymer to make a steady chemical bonding and then adding the opposite initiator. It improves stress transfer by making sure that the filler particles are evenly spread throughout the polymer milieu and by swelling the contact between the filler and polymer in the finished composite [46]. These are the primary benefits of in-situ polymerization: (a) It is easier to control the filler's distribution and interaction with the polymer's surface. (b) High-filled composites may be cast-off as a master batch and melt-mixed with other polymers to generate comparable composites, and (c) they might be utilized to manufacture high-fill and ultra-superior relative molecular mass nanocomposites. As it does not involve using lots of organic solvents, it is better for the planet than solution intercalation [46, 78]. However, graphene-based polymer nanocomposites may have their mechanical,

electrical, and thermal characteristics vastly improved by in-situ polymerization. By reacting with the polymer, the functionalized graphene forms a chemical connection at the interface that is both robust and long-lasting. The surface of graphene oxide is abundant in oxygen-containing functional groups, so polymers are typically selected whose monomers or pre-polymers can form stable chemical bonds with these oxygen-containing functional groups, like polyimide, polyurethane, epoxy resin, polyaniline, and polyvinyl alcohol. Polyaniline (PANI) and graphene oxide (GO) films remained made via in-situ polymerization by Zhu and his co-workers [79]. With impressive water dispersibility qualities and a beneficial synergistic impact on anti-corrosion performance, the produced PANI-GO nanocomposite material impressed. In addition, the coating layer's ability to prevent water penetration increases, which may serve as a kind of electro-active defense. Zhu et al. [80] have cast-off an in-situ polymerization method to manufacture a GO-polypyrrole (PPy) nanocomposite flick. Waterborne epoxy (WEP) coatings were shown to be more corrosion-resistant after being coated with this layer. Passivation by conductive PPy and the impermeable property of graphene oxide sheets are both present in the GO-PPy nanocomposites that were made. As the first step of in-situ inter-calative polymerization, graphene or altered graphene is stretched in the liquid monomer. Typically, polymerization instigates with the addition of an appropriate originator, followed by the application of heat or radiation [81, 82]. The various composites including polystyrene (PS)–graphene [83], polymethylmethacrylate (PMMA)-based expanded graphite (EG) [84], polystyrene sulfonate (PSS), polyimide (PI), and polyethylene terephthalate (PET)-based layer double hydroxide (LDH) [85–87] have been successfully reported by using this technique.

In this chapter, we have reported many strategies used in the literature to produce graphene and characterize its properties. Camphor, graphitic oxide, nanodiamonds, and silicon carbide are only a few of the precursors that have been inspected aimed at their possible usage in the production of graphene. Graphene aqueous dispersals may be manufactured using these methods. A new route for producing graphene using the hydrothermal method, cryo-milling, and lyophilization has been described. The exfoliation of graphene sheets into individual layers has been achieved by a variety of methods, including heat exfoliation and ultrasonication. In addition, the numerous characterization techniques used to verify the filler's nanostructure have been discussed. As a result of Geim and his co-worker's (2004) successful isolation of graphene, many methods for its production have been uncovered [88]. Scotch tape was proposed as a viable option for physically exfoliating graphite to directly create graphene. A piece of graphite was taped together using this method. Repeated folding and peeling of the tape produced progressively thinner layers of graphite. Finally, a single sheet of carbon called graphene is created by this process. CVD, chemical exfoliation, carbon nanotubes (slicing), and the direct sonication of carbon sheets are only a few of the methods shown in the many research studies to produce graphene. Tkalya et al. [89] created dispersions (aqueous) of graphene by oxidation and exfoliation of graphite, trailed by lessening in the occurrence of a surfactant. Graphite oxide was manufactured using a method similar to that developed by Hummer and

used for many years. The Sonic Vibracell VC750, which has a horn with a cylindrical tip, was used to exfoliate the graphene oxide (GO). The reduction procedure, which used hydrazine, took 72 h, and was conducted at a temperature of 120 °C. GO platelets were characterized via atomic force microscopy (AFM). The majority of the analyzed platelets had thicknesses of less than 1 nm or two or three atomic layers. The results confirmed the efficacy of sonic exfoliation and another case of graphene production using a more conventional hydrothermal method. Hummer's method successfully produced graphite oxide, an intermediate in the manufacture of graphene. Graphite oxide went through a series of chemical reactions to become GO. Sonicating an uneven mixture of GO and water, then reducing it with hydrazine hydrate, produced reduced GO. There are two techniques were employed to investigate the structure of graphene: XRD and FTIR spectroscopy. Reducing GO led to the formation of graphene (GR) sheets, as revealed by the presence of characteristic FTIR signals indicating the formation of the sp^2 carbon structure [90]. Pure graphite oxide was synthesized from natural flake graphite powder using Hummer's method. Boiling tetra-ethylene glycol (TEG) was used to dissolve the resultant graphite oxide.

Microwave-assisted solvothermal (MW-ST) reduction was utilized at 300˚C to lessen the yellowish-brown colloidal suspension. Indicating that graphite oxide was successfully reduced to graphene nanosheets (GNS) and the solution generated during the reduction process had a dark black hue [91]. X-ray photoelectron spectroscopy (XPS) measurements showed that GO had a higher oxygen concentration than graphene did, at 30.2% against 8.3%. These findings agreed with those obtained using the hydrazine reduction technique [92, 93]. To add insult to injury, the process was conducted in an alkaline medium at a relatively low temperature of around 180 °C. The process caused a quick change in color from yellow to brown then black which indicates that the −ve charged oxygen functional groups of graphite oxide were swiftly deoxygenated. In order to make graphite oxide, a variant of Hummer's method was utilized. Ultrasonic exfoliation was used to create GO. To produce aqueous graphene dispersion, water, hydrazine, and ammonia solutions were mixed chemically together. SEM and TEM pictures were used to examine the micrograph of GR sheets. They exhibited that 2D structures can be made thermodynamically stable by bending, and they did it by scrolling and entwining GR sheets. The success of the successive exfoliation and reduction of graphite to create graphene is shown here. According to the XRD form, the inter-planar spacing of graphene (0.36 nm) is greater than that of graphite (0.34 nm) [94]. It has been shown that the random orientation (turbostratic) of the GR sheets caused by exfoliation is related to the size of the inter-planar spacing and the resulting widening trend [95]. The results of X-ray diffraction (XRD) [96] on graphene samples made this way are the same as those made by chemical reduction. GNS was made by applying heat exfoliation and chemical reduction to graphite oxide made using the Staudenmaier process [97]. McAllister et al. [98] have previously shown that a temperature of roughly 1050 °C is enough for thermal exfoliation and an in-situ decrease in GO during this method. The XRD peaks of GO, pure graphite, and graphene were compared to prove that graphene was synthesized. Ripples in the graphene layer plane were perceived in the TEM image, a signature of the material due to its thermal variability [99]. GO

was synthesized from graphite by a variation of Hummer's method. Using hydrazine hydrate as a reductant, graphene was manufactured out of GO [100]. To create the exfoliated GO nanosheets, graphene oxide was either subjected to a solvent exfoliation or a heat exfoliation method. The hydrophilicity of graphite oxide makes solvent exfoliation possible, since water molecules may be introduced between the stacked layers. Mechanical exfoliation, accomplished by ultrasonication or constant stirring, was used to fabricate GO sheets. The resulting graphene oxide (GO) nanosheets were reduced using reducing chemicals like hydrazine hydrate to create reduced graphene oxide (RGO) or graphene [101]. For instance, Patole and his co-workers [102] have suggested the process of creating thermally expanded graphene (EG) from expandable graphite, as seen in Fig. 10.2. The procedure was supported in a chemical vapor deposition apparatus. The size, composition, and structure of EG and GR have been investigated using X-ray diffraction, SEM, and TEM.

In the SEM micrographs, there are several graphene layers were seen in the EG. After being subjected to greater temperatures, the EG samples were shown to have a reduced number of GR layers. Raman spectroscopy findings reveal that graphene has both G and 2D bands. Most graphene 2D bands have a prominent peak at roughly 2670 cm^{-1} [103]. When graphene sheet thickness declines, so does the intensity of the D band. Raman spectroscopy's G, D, and 2D bands provide striking visual representations of the graphene structure's sp^2 carbon atoms. We adapted Hummer's method, using EG as a starting point. Lyophilization and freeze-drying were used to create GNS. Many researchers have employed lyophilization procedures to create

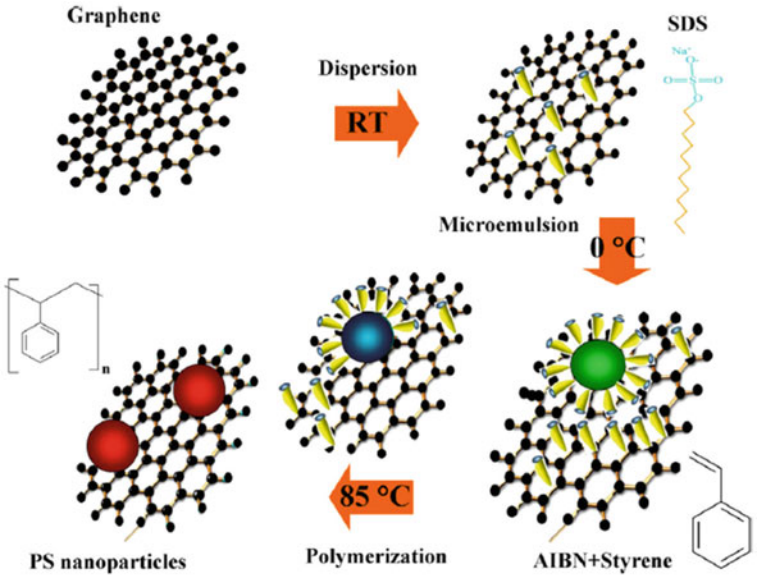

Fig. 10.2 Graphene sheets are gradually modified using PS nanoparticles [102]. Adapted with permission from Ref. [102] Copyright (2010) (Elsevier)

cellulose nano-whiskers. These nano-whisker powders may be easily redistributed in organic environments due to their low van der Waals interactions and loose packing [104, 105]. Using the same method, GNS powders were produced and found to be easily dispersed in solvents for further functionalization. It was found that the resulting GNS granules in this situation were airy and light [106–109]. Core-level-shifts X-ray photoelectron spectroscopy analysis confirmed that graphite oxide and GNS had been decreased. The GNS XRD pattern did not exhibit any peaks, in contrast to graphite oxide's pattern, which included a significant peak at 12 °C. With the use of AFM measurements, it was found that the GNS had fully exfoliated [110]. Chaturvedi et al. [111] used a powerful oxidizing chemical to treat graphite powder before ultrasonic processing in a volatile solvent. Thermal shockwave therapy was used to lessen according to the FTIR spectral task of GR, which exhibited a peak at 1628 cm^{-1}, consistent with the unoxidized graphite realms, GR was not reduced to zero after being subjected to thermal shock treatment. Analogous findings were also reported by Che et al. [112]. Mechanical exfoliation of graphite on an SU-8 exterior yielded graphene with tailor-made atomic layer thicknesses and orientations. Raman spectroscopy was used to pinpoint the monolayer in graphene [113]. Graphite oxide was created by the response of graphite with H_2SO_4, HNO_3, and potassium chlorate. For this procedure, we used a quartz tube with a rubber stopper and a sealed end. After a quick flush by argon gas via the elastic plug, the tube was proximately heated to roughly 1050 °C in a conduit incinerator. To make GO, graphite was imperiled to an adapted Staudenmaier procedure. The resultant graphite oxide was exfoliated into GO nanosheets using ultrasonics. The resulting nanosheets were then treated with ammonia and glucose in the appropriate proportions, therefore lowering GO. Ultraviolet–visible spectroscopy (UV–vis) was measured to confirm the lowering of GO with glucose. The disappearance of the C 1/4 O peak indicates a decrease in GO. Once GO was reduced, the conjugated C–C bond could once again exist, and this change influenced a redistribution of the 14-C bond's peak. According to Liu et al. [114], RGO was synthesized from GO.

In this case, hydrazine monohydrate was included in the last stages of preparation for the RGO-polyaniline (PANI) nanomaterial. GO production has been improved by revising Hummer's methodology [115]. With this method, $NaNO_3$ was removed, while $KMnO_4$ concentration was raised, a change inspired by Hummer's method. This reaction, which produced graphite oxide, was agreed out using a solution of sulfuric acid and hydrogen phosphate. The graphite oxide produced by this process was more oxidized than that produced by Hummer's technique. Thermal reduction at 200 °C for 30 min was used to transform the GO into RGO. The width of the RGO sheets was found to be 1.5 nm using AFM. Additionally, 2D thin sheets of RGO could be seen in SEM images [116]. Zeng et al. [117, 118] reported the synthesis of graphite oxide using a variation of Hummer's technique. Resin-grafted graphite oxide (RGO) was made by further sonicating graphite oxide and then reducing it with hydrazine monohydrate.

There was a significant difference in the BET surface area between camphor, graphite, and diamond samples. It was found that the samples could take in up to 3% by weight of hydrogen. Graphene with a specific surface area of 156 $m^2\ g^{-1}$ was

found to absorb just 0.4% of the hydrogen; it was subjected to in a separate study. In a simple test, the amount that a commercial graphite intercalation compound grew when it was heated was measured. The EG intercalation compound was mixed with ultrasonic waves in tetrahydrofuran (THF) for 60 min to help it spread out. Sonication resulted in the formation of GnPs with a thickness of 3.57 and 0.50 nm, respectively. Researchers have seen a potential trend toward using GnPs instead of CNTs for making polymer nanocomposite materials [119]. Table 10.1 summarizes the methods used to create graphene-based polymer nanocomposites as well as their benefits and limitations.

Table 10.1 Graphene-polymer nanocomposites: various preparative methods

Different techniques	Techniques used for the preparation of graphene-polymer nanocomposites	Benefits	Limitations
Solution mixing technique	Mechanical mixing, magnetic agitation, or large energy sonication is used to combine the graphene-solvent mixture with the polymer solution, and in the end, evaporating the solvent yields a composite	Dispersed graphene oxide composites	Eliminating solvents is a major problem
In-situ polymerization technique	By reacting monomers or pre-polymers with graphene and graphene-based polymeric composites can be made	Consistently distributed composites with enhanced characteristics	The viscosity of polymerized materials tends to increase during the process, making them difficult to manipulate and reducing their load fraction. Evaporating away the solvent is a challenge
Melt blending	Graphene and polymer mixing facilitated by elevated temperature	Sustainable, cheap, and amenable to industrial-scale production	The large shear stress may diminish the graphene aspect ratios, which would prohibit the composites from achieving their ideal minimum percolation threshold and good electrical conductivity

10.4 Graphene-Filled Different Polymer Composites

Several studies on polymer nanocomposites using various nanofillers have been published. Nonetheless, additional study into graphene-based nanocomposites for high-performance polymers is required. Graphene's usefulness as a nanofiller is demonstrated through the use of a wide variety of polymeric systems. They include epoxy, polystyrene (PS), polyaniline (PANI), polyurethane (PU), polyvinylidene fluoride (PVDF), Nafion, polycarbonate (PC), polyethylene terephthalate (PET), etc. Several academic and industrial researchers have been developing novel polymer-graphene nanocomposites for a variety of applications and may benefit from the subsequent discussion and details on graphene-based polymer nanomaterials.

10.4.1 Epoxy-Graphene Nanocomposites

Epoxy composites containing graphene oxide sheets have their thermal expansion measured using a thermo-mechanical analyzer. The heat conductivity of the epoxy resin was further reduced by the addition of graphene sheets. The embellishments of only 1% GO improved the heat conductivity of epoxy resins as much as filling them with 1% SWNT. The heat conductivity of an epoxy resin encumbered with GO at a 5 wt% was 1 W/mK, which is four-fold greater in contrast with the conductivity of raw epoxy resin. The values stated in the literature are strengthened by these findings. However, 20 wt% of GO, according to the research, might boost thermal conductivity to 6.44 W/mK. According to our findings, the graphene composite shows promise as a heat-conducting thermal interface material. Below the glass transition temperature, thermal extension related to experiments of graphene composites showed a similar influence of the SWNTs on the bulk CTEs (T_g). As compared to normal epoxy resin, which has a CTE of around 8.2 105 C1, epoxy composites containing 5 wt% graphite exhibit a decrease in CTE below T_g of 31.7%. The epoxy/graphene compounds have been fabricated on-site, and EMI shielding studies were conducted on them [120]. The critical phenomena of the percolation threshold in epoxy-graphene composites are described by the DC conductivity,

$$m = h(c)\, t\ (1), \tag{10.1}$$

where the parameters are interchangeable good agreement is found between the conductivity of polymer-graphene compounds and the percolation behavior perceived by Eq. (10.1). The data-fitting procedure yielded a percolation threshold of $c = 0.52$ vol%. Other two-dimensional fillers and an isocyanate-modified PS-based GO nanocomposite also achieved a low percolation threshold [121]. This occurred because the graphene-based sheets were evenly distributed inside the epoxy matrix and had a high aspect ratio. When a consistent graphene-based sheet network was constructed conducting in nature in the sequestering epoxy matrix, the

EMI-defending efficacy improved by enhancing graphene loading over the whole frequency assortment. However, the epoxy-based graphene compounds with a 15% graphene load attained the desired value (20 dB) for an EMI-defending composite. The results showed that polymer-graphene composite material could be used in manufacturing as light, operative composites to block electromagnetic radiation. Epoxy-graphene composites have been made using in-situ polymerization, and their ability to block EMI is evaluated [120, 122]. Graphene loading improved EMI shielding performance across the board. Thus, epoxy-graphene composite materials might be utilized as efficient, lightweight materials for protecting electronic equipment from electromagnetic radiation. We utilized a thermo-mechanical analyzer to determine the thermal expansion of epoxy composites reinforced with graphene oxide sheets [123]. The graphene slips were able to greatly upsurge the heat conductivity of the epoxy resin, which was previously quite weak. An epoxy resin filled with 5% GO composites has four times the heat conductivity of an unfilled epoxy resin [124]. Heat may be dissipated via the use of graphene composites and other thermal interface materials.

10.4.2 Polystyrene (PS)–Graphene Nanocomposites

The fabrication of polystyrene (PS)-based-isocyanate-modified graphene composites in N, N dimethylformamide (DMF) as solvent through a solution mixing approach The composites were reduced with dimethyl hydrazine for 24 h at 80˚C. To precipitate the composites, a DMF solution was added very slowly to a very huge capacity of violently stirring methanol (10:1 regarding the bulk of DMF cast-off). It seemed that almost all of the composites were filled with graphene sheets, despite only having a filler loading of 2.4% vol (found in SEM images). The electrical conductivity percolation threshold in PS with 0.1 vol.% GO was achieved. As graphene is so uniformly distributed and has such an enormously superior aspect ratio, it exhibits a percolation, i.e., three times less compared to that seen for any other two-dimensional filler [125]. Thin films loaded at around 0.15 vol.% with the composites met the antistatic criterion for conductivity (106 S m^{-1}), which is rather high. The value increased significantly between 0.4 and 1% of the load. The material's electric conduction varied from 0.1 to 1 Sm^{-1} at 2.5 vol. PS/GNPIL materials are developed in a manner analogous to the development of PS/graphene adapted with isocyanate. Compression-molded thin sheets were used to test the composite sample for electrical conductivity and thermal stability (2 mm).

Pure PS has a conductivity of around 1014 S/m when measured using a four-probe system. Adding 0.38 vol.% GNPIL significantly raised the electrical conductivity of the PS matrix to 5.77 S m1. In this article, the thermal stability of pure polystyrene is contrasted with that of the PS/GNPC8P composite material. The 2nd-step deprivation temperature of the PS-GNPC8P composite was almost 50 °C higher compared to pure PS. These point to a robust connection among the polymer matrix and GNPC8P at the boundary, which might slow down the movement of polymer shackles in the

proximity of contact which upsurge the nanocomposites' resistance to heat. Eda et al. [126] used a solution mixing method to produce PS-FGS thin films composite exhibit semiconducting behavior. The thin film displayed an ambipolar field effect. The composite thin films' 1–24 Sm^{-1} electrical conductivity was in close pact with the known standards for bulk composites. During further cooling, the conduction of the reedy coatings increased somewhat once the temperature had fallen to about 50 K. Thin films of reduced graphene oxide [128] and graphitic flakes [127] exhibited the same peculiar behavior. Below 50 K, electron–phonon scattering may limit carrier mobility. Nevertheless, the composite material shifts from n-type to p-type as the temperature increases. Each FGS and sheet-to-sheet connection has a flaw that makes it hard for carriers to move freely. The performance gap between organic and inorganic devices is expected to close as material parameters and reduction conditions are optimized. Hu and his co-workers [129] recently developed in-situ emulsion polymerization techniques used in the production of PS-graphene nanosheet (GNS) nanocomposites. The creation of PS-GNS nanocomposites is shown in simplified form in the diagram below. It was discovered that polystyrene microspheres ranging in size from 90 to 150 nm were embedded in the graphene superficially, predominantly in the crevices between the slanted nanofilms. This demonstrates the compatibility between PS microspheres and GNS, which allows for nanosized dispersion to be produced without further surface treatment. When pure GNS (0.37 nm) was put next to PS/GNS nanocomposites (0.41 nm), the distance between the layers grew. To reduce the strength of the van der Waals forces and increase the inter-planar distance between the slanted nanosheets, PS microspheres may be attached to the edges of the nanosheets. Raman spectra of pure GNS nanocomposites and PS/GNS hybrids are shown. It was determined that pure GNS has two distinct properties, the D band at 1331 cm^{-1} and the G band at 1594 cm^{-1}. The peak intensity ratio, I(D)/I(G), for the PS-GNS nanocomposites, was 1.156. As a result, it is possible that the chemical grafting of polymers to the GNS surface is facilitated by the presence of localized areas of sp^3 blemishes within the sp^2 network of carbon [130]. Nanocomposites have 100 °C higher thermal stability than pure PS. Increased T_g may be traced back to a strong interaction between the polymer matrix PS and GNS, as seen below. At a GNS content of 2.0 wt%, the electrical conductivity of the PS/GNS nanocomposites was found to be 2.9 102 S m1. It was, however, mentioned that pure PS had a conductivity of around 1.0 1010 S m1 [131]. It was recently reported that a nanostructured poly(styrene–isoprene-styrene) block copolymer had PS domains containing functionalized graphene sheets (FGS) (SIS). Analysis of AFM images reveals that poly(styrene-b-isoprene-b-styrene) is made up of well-ordered, spherical PS block domains that are perpendicular to the free surface (SIS). Cylindrical PS domains have been found dispersed perpendicular and corresponding to the free exterior in SIS and FGS composites. Mean diameters of 20 nm (and their long-range order) were found in both the clean matrix and the cylindrical domains of the nanocomposites. T_g for the PS block increased from 78 °C for pure SIS to 84 degrees Celsius for the SIS/FGS composite, whereas the T_g for the PI block stayed relatively constant at around 58 degrees Celsius for both materials. T_g increases because chain mobility in PS domains is impeded. The researchers claim that by incorporating 2D particles into BC, BC is

endowed with robust electrical properties that are essential for optoelectronic uses. The solution blending method using DMF as the solvent was used to produce modified graphene composites, including PS and isocyanate [132]. The compounds were coagulated by gradually adding DMF to a large volume of CH_3OH. These composites seemed to be nearly filled using a graphene sheet, although they contained just 2.4% filler by volume. The conductivity of a composite material may be understood as a function of the volumetric proportion of filler loading. By using a similar method, Liu et al. [133] were able to produce a PS-ionic liquid-functionalized graphene composite that displayed enhanced electrical conductivity compared to unmodified PS. Functionalized graphene sheet (FGS) materials have been developed by solution amalgamation [126]. Thin layers of semiconducting composites exhibited the interfacial field effect. The thin coatings' conductivity decreased at temperatures as high as 50 K and then slightly increased with subsequent cooling. These results were also seen in thin films of diminished GO and graphitic flakes [128, 134]. For their nanocomposites, Hu and his research team [135] used in-situ emulsion polymerization to make graphene nanosheets (GNS) materials. Including PS microspheres with GNS may lead to non-sized dispersion without the need for any further surface preparation. The nanocomposite was 100 ˚C more stable at high temperatures than pristine PS. The electric conduction process of the PS-GNS nanomaterial is greatly more sophisticated than that of pristine PS.

10.4.3 Polyaniline (PANI)-Graphene Nanocomposites

To synthesize PANI-based graphene composite paper, aniline was electropolymerized in-situ on graphene paper (GPCP) [136]. A three-electrode anodic electro-polymerization cell was used to conduct the polymerization. Graphite paper was used as the active electrode, while a Pt plate was used as the counter electrode and a standard calomel electrode (SCE) as the reference electrode. The electrolyte was composed of aniline and sulphuric acid (at a concentration of 0.5 m) (0.05 M). During a long length of time, PANI was electro-polymerized in situ on graphene paper using a constant potential of 0.75 V against the SCE (60, 300, and 900 s). However, the GPCP's morphology was studied with electron energy loss spectroscopy (EELS). The presence of homogeneous PANI coatings on a single graphene sheet was demonstrated by the identification of nitrogen, carbon, and oxygen that were uniformly distributed throughout the whole surface of the PANI-graphene sheet. In contrast to the regular arrangement of PANI on each 2D graphene, the 3D structure of GPCP is inhomogeneous. The results from cyclic voltammetry (CV) on graphene paper (GP) and graphene-enhanced carbon nanotubes (GPCP). It is because of the transition between quinone and hydroquinone classes, GP has a single redox peak. It is observed that the two groups of redox peaks were seen in the GPCP, indicating the presence of pseudo-capacitive PANI in the composites [136].

The redox characteristics of GP and GPCP are examined in a Nyquist plot (Fig. 10.3a). The higher resistance is owing to the increased concentration of GPCP,

and this may be owing to the build-up of poorer conducting PANI. On the other hand, GPCP demonstrated much higher cycle stability than GP (Fig. 10.3b). An excellent composite of PANI-graphene electrodes was developed using a spin coating method [136, 137]. However, a pure aqueous dispersion of GO sheets was deposited via a deep coating method on a quartz substrate and then thermally reduced to create a graphene layer. The graphene sheets were then spin-coated with a dark blue PANI solution in NMP. According to morphological tests, the PANI-graphene electrodes had far smoother surfaces than that of the indium tin oxide (ITO) or PANI-ITO electrodes. The current density of the CV at the PANI-ITO electrodes reduced dramatically after being subjected to 100 cycles at 20 mV s^{-1} in 1 mol L^{-1} H_2SO_4, and the potential change among the oxidation and reduction increased from 87 to 106 mV. When applied to a PANI-graphene electrode, the same process showed negligible impact on the material's overall qualities. So, when making electrochromic devices, the PANI-graphene electrode is better than an ITO electrode. After a few cycles of potential switching, the ITO electrode's performance significantly decreased, despite its initial high optical contrast and short switching time. However, when the voltage was altered, the electrochromic devices using graphene electrodes showed only a slight decrease in performance. The PANI-GNS-CNT composite was fabricated using in-situ polymerization [136, 138]. Electrodes were made by dissolving electroactive materials like carbon black and polytetrafluoroethylene (PTFE) in ethanol. The resulting slurry was spread with a spatula on a nickel substrate before being baked at 100 °C for 12 h under a vacuum. The specific capacitance of the synthesized PANI composites and pure PANI is presented in Fig. 10.4 as a function of scan rates. The PANI-GNS-CNT composites greatly outperformed pure PANI and PANI-CNT composites in terms of specific capacitance. An increased specific capacitance was attributed to a synergistic effect between GNS and PANI [136, 139].

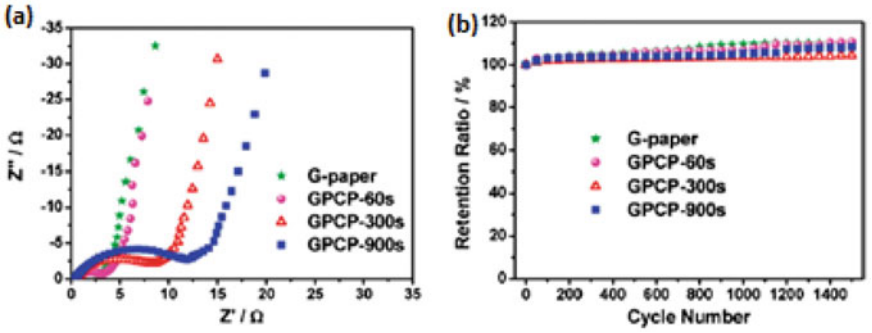

Fig. 10.3 Comparison of cyclic voltammograms captured in 1 M H_2SO_4 at rates ranging from 2 to 20 mV/s (**a**). The Nyquist plots of the G-paper and GPCP (60 s, 300 s, and 900 s) (**b**), with stability at 50 mV/s cycling [136]. Adapted with permission from Ref. [136] Copyright (2010) (Elsevier)

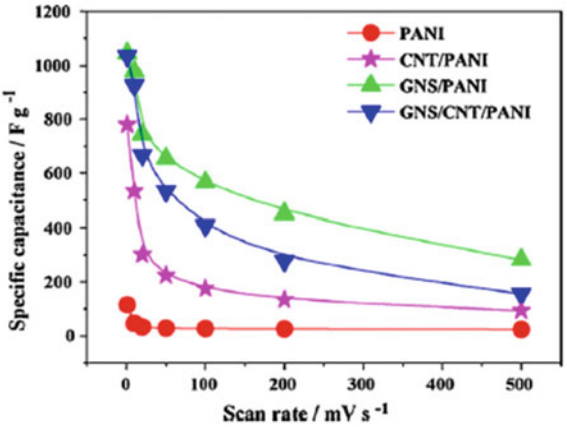

Fig. 10.4 Capacitance data at varying scan rates for polyaniline, carbon nanotube polyaniline, graphene nanosheets polyaniline, and graphene nanosheet carbon nanotube polyaniline. The GNS-PANI electrode material was found to be superior since it had the largest specific capacitance [136]. Adapted with permission from Ref. [136] Copyright (2010) (Elsevier)

10.4.4 Nafion-Graphene Nanocomposites

Graphene and Nafion were combined in a solution to create an electrode modified with tris(2,2-bipyridyl) ruthenium (II) ($Ru(bpy)_3^{2+}$) [140]. The electrode was soaked for 30 min in a 1 M $Ru(bpy)_3^{2+}$ solution to produce a $Ru(bpy)^{3+}$ modified electrode. The cyclic voltammetry (CV) of the modified Nafion-graphene electrode suggests that graphene's conductivity improves in electron transport. Electrochemical catalysis of TPA oxidation by the $Ru(bpy)_3^{2+}$)-Nafion-graphene composite film is demonstrated by an increase in the anodic peak current upon addition of TPA. With the modified electrode, oxalate ions were detected with high sensitivity, selectivity, and stability. Graphene-Nafion-tris(2,21-bipyridyl)ruthenium(II) ($Ru(bpy)_3]^{2+}$) Graphene and Nafion were combined in a solvent to create specialized electrodes [141, 142]. The synthesized electrode was subsequently exposed to 1 M $[Ru(bpy)_3]^{2+}$ solution. The responsiveness, selectivity, and stability of the modified electrode significantly increased.

10.4.5 Poly(Vinyl Alcohol) (PVA)-Graphene Nanocomposites

Liang and his co-workers [143] have reported that the poly(vinyl alcohol) (PVA)-based graphene nanocomposites comprise GO as fillers, PVA as a polymer matrix, and water as the processing solvent. The synthesized GO and PVA-based GO nanocomposites were analyzed by X-ray diffraction studies (as shown in Fig. 10.5). It was found that the peak at 20.9° that crystallized matched the GO and suggested that the GO had exfoliated into individual sheets.

It is reported that the PVA-based graphene nanocomposites performed better mechanically than pure PVA. However, the tensile strength was observed to increase by 76% (from 49.9 to 87.6 MPa) and Young's modulus by 62% (from 2.13 to

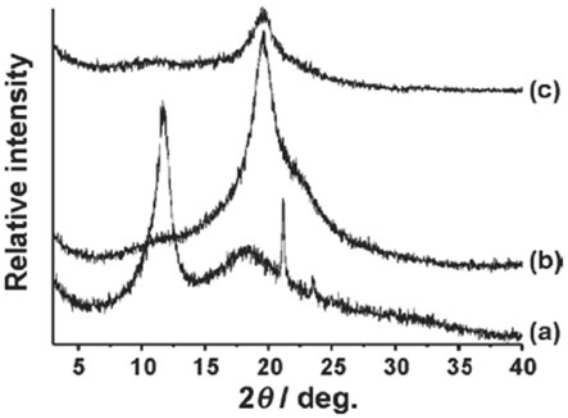

Fig. 10.5 X-ray diffraction (XRD) patterns of **a** graphene oxide (GO), **b** graphene-polyvinyl alcohol (PVA) nanocomposite with 0.5 wt% of GO, and **c** neat PVA [143]. Adapted with permission from Ref. [143] Copyright (2009) (Willey)

3.45 GPa), when the GO loading was increased from 0% to 0.7 wt% (0.41 vol.%). There are various factors for the molecular-level dispersion of graphene sheets in the PVA matrix and their strong interfacial adhesion owing to their H-bonding with the PVA matrix. The incorporation of 0.7 wt% of GO into PVA-graphene nanocomposites corresponded with a rise in glass transition temperature (T_g) from 37.5 to 40.8 °C. This raise in T_g may be due to the H-bonding of graphene and PVA matrix. It has been found that DSC can be used to detect the hydrogen bonding of graphene and PVA. These nanocomposites have better crystallographic and thermal stability than neat PVA. Further, these graphene nanosheets and extensively exfoliated PVA-based nanocomposites were made using a facial aqueous solution [149]. When graphene nanosheets were mixed into the PVA matrix, the resulting composites showed increased strength. A tensile strength of 42 MPa was demonstrated by the composite containing 1.8% graphene by volume, an increase of 150% over the corresponding pure PVA sample. The addition of more graphene relatively significantly raised the tensile strength from 42 to 43 MPa. When graphene loading was increased, the composites' elongation at break reduced dramatically and unexpectedly. The presence of 1.8 vol. % graphene reduced the elongation at break from 220% in the neat sample to 98% in the composite. The study found that graphene-based nanocomposites have a high aspect ratio and well contact with the polymer matrix slowed down the chain's mobility.

10.4.6 Polyurethane (PU)-Graphene Nanocomposites

Nanocomposites made from FGS and water-based polyurethane were produced using an in-situ approach (WPU). The morphological analysis of the nanocomposite showed that the FGS particles were spread out evenly over the WPU matrix. These

nanocomposites have superior electrical conductivity owing to their uniform distribution of FGS particles throughout the WPU matrix. However, the percolation threshold was reached at a loading of only 2% FGS. Once an electrically conducting channel formed in the polymer matrix, the electrical conductivity of the polymer changed. Lee and his co-workers have made FGS-WPU nanocomposites that have a higher conductivity [144]. A DSC study found that adding FGS to nanocomposites raises both the melting temperature and the heat of fusion (H_m) of the soft segment of WPU. In contrast, hard segment crystallinity decreased with increasing FGS loading in the nanocomposites.

Besides, three different nanocomposites were developed by Liang et al. through the use of solution mixtures. They used graphene that had been treated with isocyanate, sulfonate, or reduction as the nanofiller and thermoplastic polyurethane (TPU) as the matrix polymer [145]. According to TGA testing, the thermal breakdown rate of TPU nanocomposites made from reduced and sulfonated graphene was much lower than that of isocyanate-modified graphene. Graphene sheets that have been sulfonated have fewer functional groups attached than graphene that has been changed with isocyanate. The infrared-triggered actuation performance of TPU-graphene nanocomposites comprising 1 wt.% sulfonated graphene was fascinating and durable. When exposed to infrared light, this infrared-responsive nanocomposite decreased and rapidly raised a 21.6 g weight of 3.1 cm (0.21 N). There are several cycling tests yielded a maximum energy density of 0.40 Jg^{-1}. Furthermore, the isocyanate-modified graphene-TPU nanocomposites exhibited a poor shape recovery rate and IR-triggered actuation (Fig. 10.6), whereas TPU-sulfonated graphene nanocomposites had improved electrical and mechanical performances. Nanocomposites made with 1% TPU-sulfonated graphene had their tensile strength (100% strain) rise by 75%, and their Young's modulus goes up by 120%. This improvement in mechanical characteristics may be due to the uniform dispersion of graphene in the polymer matrix.

10.4.7 Poly(Vinylidene Fluoride) (PVDF)-Graphene Nanocomposites

Graphene oxide and expanded graphite (EG) were used in a solution processing and compression molding process to create a PVDF based on functionalized graphene sheets (FGS) [146]. The structure and thermal stability of the composites were analyzed through X-ray diffraction and dynamic scanning calorimetric technique. However, it is observed that modified composites have superior mechanical performance than those of pristine polymer and unmodified ones. It is noticed that at 25 °C, pure PVDF had a storage modulus of 1275 MPa, but adding 2 wt% FGS or EG raised it to 1859 or 1739 MPa. Further, with the incorporation of 4 wt% filler into the PVDF matrix, the storage modulus rises to 2460 and 2695 MPa, respectively. The DMA results demonstrated that the nanofiller's reinforcing impact contributed to the

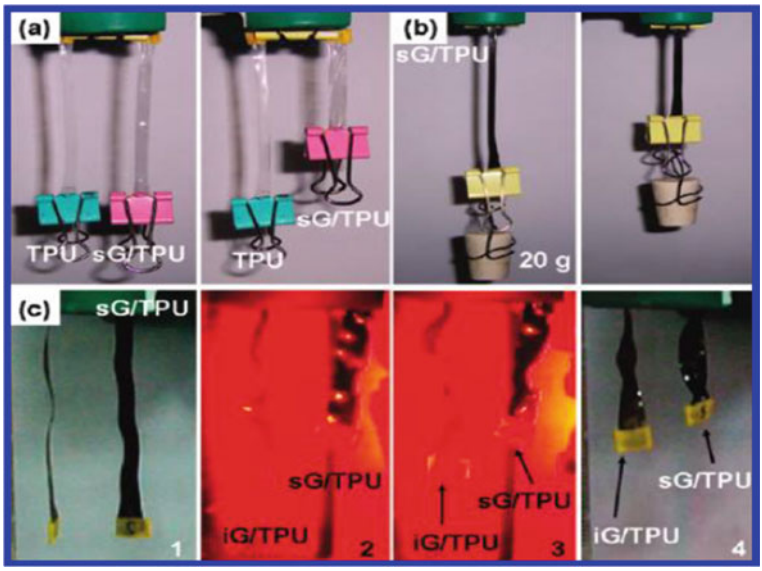

Fig. 10.6 Infrared optical pictures of nanocomposites using graphene as the active material [145]. Adapted with permission from Ref. [145] Copyright (2009) (American Chemical Society)

nanocomposites' improved Tg. At a loading of 5% EG in PVDF-FGS composites and 2% FGS in PVDF-EG composites, the percolation of electrical conductivity was shown to be very significant, owing to their larger aspect ratio, FGS has a lower percolation threshold and a better-conducting network than EG. The influence of temperature on the electrical conductivity of the PVDF-EG nanocomposites was also studied at temperatures ranging from 20 to 170 °C. This nanocomposite resistivity increased steadily with increasing temperature, increasing rapidly after the polymer melt. As the filler particles are so much farther apart at melting, they offer considerably more resistance. It was thought that nanocomposite materials could be used as positive temperature coefficient (PTC) materials because the resistivity changes by three orders of magnitude as the amount of EG changes.

10.4.8 Poly(3,4-Ethyldioxythiophene)-Graphene Nanocomposites

Using in-situ polymerization, a composite of poly (3,4-ethyl dioxythiophene) (PEDOT) and sulfonated graphene was developed [147]. This novel hybrid material has excellent transparency, electrical conductivity, outstanding flexibility, and high thermal stability, and it can be easily treated in both aqueous and organic solvents. Optical transmittances at 550 nm were found to be 96%, 76%, 51%, and

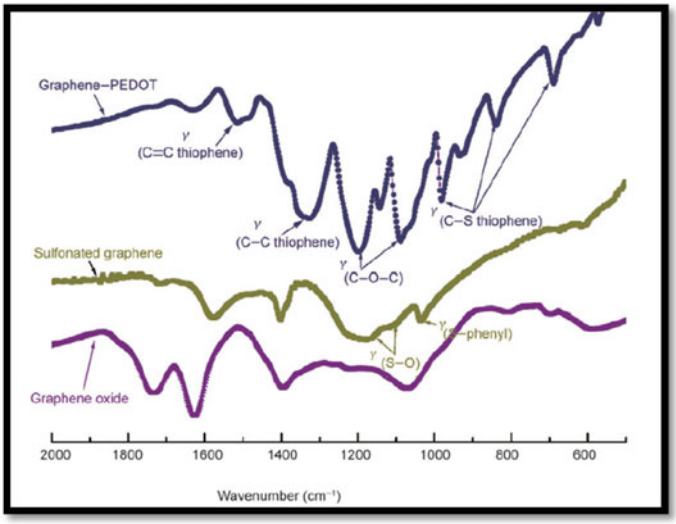

Fig. 10.7 Graphene oxide, sulfonated graphene, and graphene-PEDOT FTIR spectra [147]. Adapted with permission from Ref. [147] Copyright (2009) (Springer Nature)

36% for PEDOT-graphene films of thicknesses of 33, 58, 76, and 103 nm, respectively (Fig. 10.7). The conductivity of the composite films produced on quartz and PMMA substrates was 7 and 10.8 Sm^{-1}, respectively, regardless of the film thickness. PEDOT-graphene composites are favorable owing to their superior thermal stability. Moreover, the temperature of 297 and 325 °C, the composite material exhibits mass loss, and below 325 °C, mass loss reached roughly 19%. The PEDOT-graphene composite also showed improved thermal stability over PEDOT-PSS composites.

10.4.9 Polyethylene Terephthalate and Polycarbonate-Based Graphene Nanocomposites

Melt compounding was used to create graphene nanocomposites based on polyethylene terephthalate (PET) [148]. The morphological analysis of the nanocomposites revealed that the graphene network is composed of several thin stacks of a few sheets of monolayer graphene. The wrinkly, overlapping graphene sheets that come out of this process may have a high electrical conductivity because they connect the individual graphene sheets well and move a lot of current [149]. Melt compounding was used to make composites of polycarbonate (PC) and functionalized graphene sheets (FGS) or graphite. The structural, morphological, and rheological study of the PC-FGS composites revealed that the FGS layers were significantly exfoliated and had viscoelastic properties. After being annealed for 10,000 s, the PC-FGS composites show stiffness percolation at 1wt% to 1.5t5 of FGS loading into the PC matrix. In

contrast, a graphite loading of 3–5 wt% was sufficient to achieve this percolation. These composites with a weight percentage of (0.5 wt %) of FGS contents have interesting reversibility among solid and liquid performance, and this is impacted by prior processing. However, the electrical properties of the resultant composites with lower FGS loadings might still result in electrical conductivity percolation, in comparison with utilizing graphite filler. It has been found that PC-FGS nanocomposites have a greater tensile modulus than pure PC. Because of the FGS loading, the CTEof the composites was also greatly diminished. Graphite- and FGS-reinforced polycarbonate films were subjected to N2 and He penetration tests at 35 °C. Both enhancers have the potential to make nitrogen and helium in the air less harmful. However, FGS composites had significantly lower permeability than graphite composites. Gas molecules diffuse slower across membranes because a uniform distribution of FGS with a large aspect ratio may produce complex routes, lowering the cross-sectional area available for penetration [150].

10.5 Application of Polymer-Graphene Composites for Energy Storage Devices

In recent times, one of the most promising methods of energy storage is the super capacitor since it has a high power density, is quick to charge and discharge, and has a long cycle life. The electrodes in super capacitors would be made from a 3D graphene-based conductive structure owing to its elevated specific charge, low density, and superior surface area. The optimum electrode materials for pseudocapacitors are typically mixtures of conducting polymers (PANI and PPy) and graphene that have a high theoretical capacitance owing to their unique redox characteristics [151]. However, the conducting polymer to 3D graphene for supercapacitors stabilizes the polymer chain in the network, increases electrolyte ions' surface accessibility, minimizes their diffusion distance, and improves the composite performance [152]. The 3D graphene-based polymer nanocomposites can be created by cross-linking organic molecules with 3D graphene using a self-assembled method followed by in-situ polymerization. Liu et al. [153] also made a graphene supercapacitor that can withstand a lot of pressure. They also came up with a way to make 3D PPy-graphene (PPy-G) foam in place by cross-linking organic molecules. The good porosity, conductivity, and mechanical durability of PPy-G foam electrodes kept their CV curves and capacitive even after 1000 recorded cycles with a 50% strain. Moreover, the compact PPy sheets and pure 3D graphene have specific capacitances that are substantially lower than the discharge slope prediction of 350 F/g^{-1}. Figure 10.8 shows different application analyses of graphene, from conductive ink to chemical sensors to LEDs to composites to energy to touch screens and high-frequency electronics.

Kulkarni et al. [154] used an in-situ polymerization technique to fabricate PANI nanofibers with a diameter of 20–100 nm using a 3D graphene template. With a current density of 4 mA/cm^2, it was thought that the battery would keep 86.5%

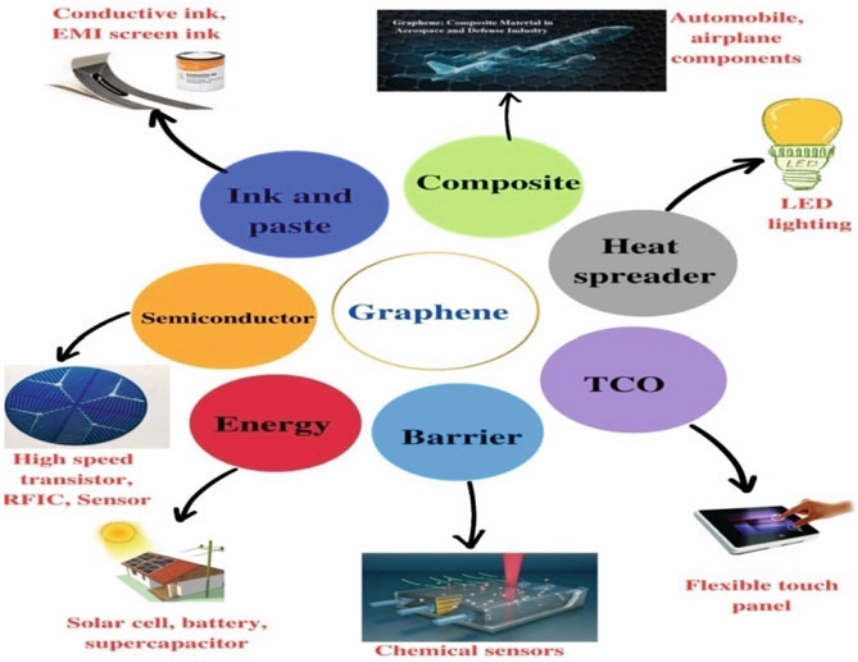

Fig. 10.8 Use of graphene-based materials in a variety of disciplines

of its original capacity after 5000 cycles of charging and discharging. The active PANI nanofibers have huge specific surface area and the graphene backbone's efficient conducting routes enhanced cycle stability and rate capability, resulting in a surprising synergistic efficiency for better super capacitive performance. When scanned from 150 to 800 mV at 10 mV s^{-1}, composite electrodes had a maximum specific capacitance of 1024 F g^{-1} in 1 M H_2SO_4. Another study that used sonication or reduction to make a 3D graphene-poly(anthraquinonyl sulfide) (PAQS) composite was conducted by Zhang et al. [155]. This composite could be used as a bendable cathode in LIBs and $NaIO_2$ batteries (SIBs) if it was put under mechanical pressure. As a result of the stacking relationship between the graphene sheets, the polymer particles (100–200 nm) were evenly dispersed across the graphene surface and enclosed within the graphene sheets. The improved composite has very good cycling stability (71.4% capacity retention after 1000 cycles at 0.5 °C) and excellent rate performance (102 mAh g^{-1} for LIBs at 20 °C and 72 mAh g^{-1} for SIBs at 5 °C). To make it easier for active polymers to react electrochemically, PAQS particles were spread out evenly and encased in 3D graphene with a porous structure that was built up in layers [156]. This allowed for reliable ion transport channels and a viable electron transport path. The microbial fuel cell (MFC) used as a bio-oxidation method is another way to turn chemical energy from organic substrates like sugar, fatty acids, and proteins into electricity [157, 158]. However, the high porosity in the

3D graphene structures allows the bacteria and a growth medium access to the inside of the electrode. Yang et al. [159] have reported that the hydrophilic conducting polymer PANI is on 3D graphene by polymerizing it. This made it easier for bacteria to stick to the surface and form biofilms [160]. Bacteria colonized the PANI-coated graphene surface and established an extensive biofilm. The middle PANI polymers acted as conductive nanowires to increase extracellular electron transport between the electrode and the microorganisms by engaging directly with the redox-active proteins on the bacterial membrane [161, 162]. It has been reported that after 150 h (Fig. 10.9a), the power density of the graphene-PANI MFC as still significantly higher than that of carbon cloth. Furthermore, the charge-transfer resistance of the graphene-PANI MFC was only around 100 (as shown in Fig. 10.9a). Moreover, the 3D graphene-PANI MFC composites reached a maximum power density of about 768 mW/m^2 (Fig. 10.9b). Figure 10.9c demonstrates that the high bacterial loading and efficient EET gave the 3D graphene-PANI anode a naturally high output power density (extracellular electron transfer). Chitosan was used as a backbone for 3D-GPNCs along with conducting polymers because it is biocompatible, can absorb, and is good for the environment. Chen et al. [162] made a 3D chitosan-vacuum-stripped graphene scaffold using a self-assembly method. The hierarchically porous structure with layered, branched macropores, mesopores, and micropores increased bacterial colonization and electron transfer from redox-active compounds. The highest power density in MFC came from a 50% graphene scaffold at 1530 mWm^{-2}, and this is 78 times more powerful than a carbon cloth anode.

Xia and his co-workers [163] have made a composite material by decorating functionalized graphene sheets with Fe_2O_3 quantum dots (QDs, 2 nm) (FGS) through a facile technique and used it as a supercapacitor electrode (as shown in Fig. 10.10). The specific capacitance of these Fe_2O_3 QDs-FGS composites in 1 M Na_2SO_4

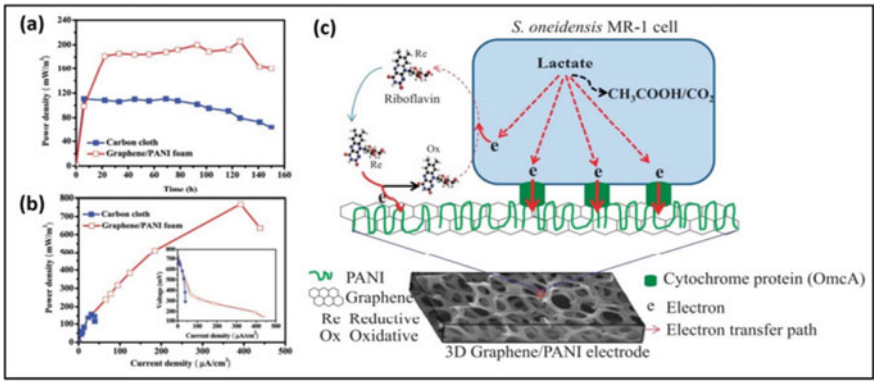

Fig. 10.9 **a** MFCs with carbon cloth or graphene-based PANI foam anodes have different power density output time courses, **b** polarization curves of the two MFC types (I-V relation inset) **c** This picture shows S. oneidensis MR-1 bacteria and a 3D graphene-PANI monolith electrode interacting with each other [162]. Adapted with permission from Ref. [162] Copyright (2012) (American Chemical Society)

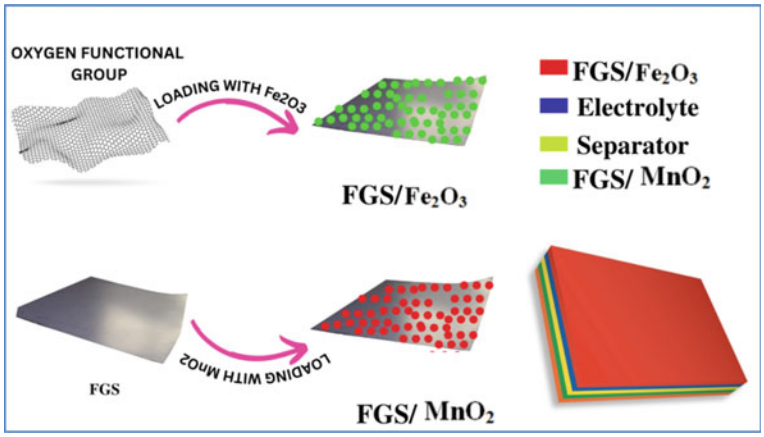

Fig. 10.10 A schematic representation of the creation of an asymmetric supercapacitor and design of the composite electrodes

between -1 and 0 V vs Ag–AgCl can reach up to 347 F/g^{-1}. The Fe_2O_3-FGS-MnO_2-FGSasymmetric supercapacitor has a power density of 100 W kg^{-1} and an energy density of 50.7 Wh kg^{-1}, and it has outstanding cycling stability.

10.6 Conclusions

Graphene research and development is progressing at a breakneck pace right now, with huge breakthroughs being made every day. Recent progress in our understanding of graphene polymer nanocomposites can be traced to the dramatic improvements in polymer properties, such as mechanical, electrical, thermal conductivity, chemical, optical, and gas impermeability, which can be made with low concentrations of filler. In this chapter, we focused on the precise incorporation of surface-functionalized graphene into different polymer matrices to realize their potential applications in fields of energy storage sectors including electronics and composite materials. The enhanced characteristics are a result of the uniform distribution of changed graphene and improved polymer-graphene compatibility via a variety of reactive functional groups on modified graphene. Graphene's emergence as viable nanofillers has ushered in a new era in the development of low-cost, high-performance composites for a wide variety of uses.

Acknowledgements The authors gratefully acknowledge the support provided by Centurion University of Technology and Management, Odisha, India, for carrying out the present research work.

Conflicts of Interest The authors declare no conflict of interest.

References

1. Okada A, Kawasumi M, Usuki A, Kojima Y, Kurauchi T, Kamigaito O (1990) Synthesis and properties of nylon-6/clay hybrids. Polymer-based molecular composites. In: MRS symposium proceedings, Pittsburgh, vol 171, pp 45–50
2. Nurazzi NM, Sabaruddin FA, Harussani MM, Kamarudin SH, Rayung M, Asyraf MRM, Khalina A (2021) Mechanical performance and applications of CNTs reinforced polymer composites-a review. Nanomater 11(9):2186
3. Wazalwar R, Sahu M, Raichur AM (2021) Mechanical properties of aerospace epoxy composites reinforced with 2D nano-fillers: current status and road to industrialization. Nanoscale Adv 3(10):2741–2776
4. Essabir H, Raji M, Bouhfid R, Qaiss AEK (2021) Hybrid nanocomposites based on graphene and nano-clay: preparation, characterization, and synergistic effect. In: Graphene and nanoparticles hybrid nanocomposites: from preparation to applications, pp 153–181
5. Bhanushali H, Amrutkar S, Mestry S, Mhaske ST (2022) Shape memory polymer nanocomposite: a review on structure–property relationship. Polym Bull 79(6):3437–3493
6. Karki S, Gohain MB, Yadav D, Ingole PG (2021) Nanocomposite and bio-nanocomposite polymeric materials/membranes development in energy and medical sector: a review. Int J Biol Macromol 193:2121–2139
7. Siwal SS, Zhang Q, Devi N, Thakur VK (2020) Carbon-based polymer nanocomposite for high-performance energy storage applications. Polymer 12(3):505
8. Benny Mattam L, Bijoy A, Abraham Thadathil D, George L, Varghese A (2022) Conducting polymers: a versatile material for biomedical applications. ChemistrySelect 7(42):e202201765
9. Kruželák J, Kvasničáková A, Hložeková K, Hudec I (2021) Progress in polymers and polymer composites used as efficient materials for EMI shielding. Nanoscale Adv 3(1):123–172
10. Shahapurkar K, Gelaw M, Tirth V, Soudagar MEM, Shahapurkar P, Mujtaba MA, Ahmed GMS (2022) Comprehensive review on polymer composites as electromagnetic interference shielding materials. Polym Polym Compos 30:1–17
11. Samsudin SS, Abdul Majid MS, MohdJamir MR, Osman AF, Jaafar M, Alshahrani HA (2022) Physical, thermal transport, and compressive properties of epoxy composite filled with graphitic-and ceramic-based thermally conductive nanofillers. Polym 14(5):1014
12. Minisha S, Vedhi C, Rajakani P (2022) Methods of graphene synthesis and graphene-based electrode material for supercapacitor applications. ECS J Solid State Sci Technol 11(11):111002
13. Sethulekshmi AS, Jayan JS, Appukutta S, Joseph K (2021) MoS_2: Advanced nanofiller for reinforcing polymer matrix. Phys E Low Dimens Syst Nanostruct 132:114716
14. Lian C, Gu Z, Zhang Y, Ma Z, Qiu H, Gu J (2021) Structural design strategies of polymer matrix composites for electromagnetic interference shielding: a review. Nano-Micro Lett 13(1):181
15. Li Y, Huang X, Zeng L, Li R, Tian H, Fu X, Zhong WH (2019) A review of the electrical and mechanical properties of carbon nanofiller-reinforced polymer composites. J Mater Sci 54:1036–1076
16. Ansari MNM, Sayem MA (2023) Microwave-assisted activated carbon: a promising class of materials for a wide range of applications. In: Radiation technologies and applications in materials science, pp 331–368
17. Hecht DS, Hu L, Irvin G (2011) Emerging transparent electrodes based on thin films of carbon nanotubes, graphene, and metallic nanostructures. Adv Mater 23(13):1482–1513
18. El-Kady MF, Shao Y, Kaner RB (2016) Graphene for batteries, supercapacitors and beyond. Nat Rev Mater 1(7):1–14
19. Kumar SSA, Bashir S, Ramesh K, Ramesh S (2021) New perspectives on graphene/graphene oxide based polymer nanocomposites for corrosion applications: the relevance of the graphene/polymer barrier coatings. Prog Org Coat 154:106215

20. Mohan VB, Lau KT, Hui D, Bhattacharyya D (2018) Graphene-based materials and their composites: a review on production, applications and product limitations. Compos B Eng 142:200–220
21. Shmavonyan G, Cheshev D, Averkiev A, Tran TH, Sheremet E (2022) Nanospectroscopy of graphene and two-dimensional atomic materials and hybrid structures. Opt Nanospectroscopy 401
22. Moharana S, Mahaling RN (2017) Silver (Ag)-Graphene oxide (GO)-Poly (vinylidene fluoride-co-hexafluoropropylene)(PVDF-HFP) nanostructured composites with high dielectric constant and low dielectric loss. Chem Phys Lett 680:31–36
23. Novoselov KS, Geim AK, Morozov SV, Jiang D, Zhang Y, Dubonos SV (2004) Electric field effect in atomically thin carbon films. Sci 306:666–669
24. Asghar F, Shakoor B, Fatima S, Munir S, Razzaq H, Naheed S, Butler IS (2022) Fabrication and prospective applications of graphene oxide-modified nanocomposites for wastewater remediation. RSC Adv 12(19):11750–11768
25. Ashraf G, Aziz A, Iftikhar T, Zhong ZT, Asif M, Chen W (2022) The roadmap of graphene-based sensors: electrochemical methods for bioanalytical applications. Biosensors 12(12):1183
26. Moharana S, Mahaling RN (2021) Enhancement investigations on dielectric and electrical properties of niobium pentoxide (Nb_2O_5) reinforced poly (vinylidene fluoride)(PVDF)-graphene oxide (GO) nanocomposite films. J Asian Ceram Soc 9(3):1183–1193
27. Nitin MS, Suresh Kumar S (2022) Ballistic performance of synergistically toughened Kevlar/epoxy composite targets reinforced with multiwalled carbon nanotubes/graphene nanofillers. Polym Compos 43(2):782–797
28. Dubey PK, Hong J, Lee K, Singh P (2023) Graphene-based materials: synthesis and applications. In: Nanomater, pp 59–84
29. Patra L, Pandey R (2022) Mechanical properties of 2D materials: a review on molecular dynamics based nanoindentation simulations. Mater Today Commun 31:103623
30. Balandin AA (2011) Thermal properties of graphene and nanostructured carbon materials. Nat Mater 10(8):569–581
31. Jung I, Dikin DA, Piner RD, Ruoff RS (2008) Tunable electrical conductivity of individual graphene oxide sheets reduced at "low" temperatures. Nano Lett 8(12):4283–4287
32. Chauhan AK, Gupta SK, Taguchi D, Manaka T, Jha P, Veerender P, Iwamoto M (2017) Enhancement of the carrier mobility of conducting polymers by formation of their graphene composites. RSC Adv 7(20):11913–11920
33. Matte HR, Subrahmanyam KS, Rao CNR (2009) Novel magnetic properties of graphene: presence of both ferromagnetic and antiferromagnetic features and other aspects. J Phys Chem C 113(23):9982–9985
34. Guo Q, Dedkov Y, Voloshina E (2020) Intercalation of Mn in graphene/Cu (111) interface: insights to the electronic and magnetic properties from theory. Sci Rep 10(1):21684
35. Geng Y, Wang SJ, Kim JK (2009) Preparation of graphite nanoplatelets and graphene sheets. J Colloid Interface Sci 336(2):592–598
36. Vacchi IA, Ménard-Moyon C, Bianco A (2017) Chemical functionalization of graphene family members. Phys Sci Rev 2(1)
37. Ioniţă M, Vlăsceanu GM, Watzlawek AA, Voicu SI, Burns JS, Iovu H (2017) Graphene and functionalized graphene: extraordinary prospects for nanobiocomposite materials. Compos B Eng 121:34–57
38. Acik M, Chabal YJ (2011) Nature of graphene edges: a review. Jpn J Appl Phys 50(7R):070101
39. NebolSin VA, Galstyan V, Silina YE (2020) Graphene oxide and its chemical nature: multistage interactions between the oxygen and graphene. Surf Interfaces 21:100763
40. Shi L, Xia W (2012) Photoredox functionalization of C-H bonds adjacent to a nitrogen atom. Chem Soc Rev 41(23):7687–7697
41. Cao Y, Osuna S, Liang Y, Haddon RC, Houk KN (2013) Diels-Alder reactions of graphene: computational predictions of products and sites of reaction. J Am Chem Soc 135(46):17643–17649

42. Guday G (2019) Surface chemistry of low-dimensional carbon materials: synthesis and functionalization of graphene. Freie Universitaet Berlin (Germany)
43. He J, Qiu D, Li Y (2020) Strategies toward aryne multifunctionalization via 1, 2-benzdiyne and benzyne. Acc Chem Res 53(2):508–519
44. Rkein B, Bigot A, Birbaum L, Manneveau M, De Paolis M, Legros J, Chataigner I (2021) Reactivity of 3-nitroindoles with electron-rich species. Chem Commun 57(1):27–44
45. Ratwani CR, Abdelkader A(2022) Self-healing by Diels-Alder cycloaddition in advanced functional polymers: a review. Prog Mater Sci, p 101001
46. Ashfaq A, Clochard MC, Coqueret X, Dispenza C, Driscoll MS, Ulański P, Al-Sheikhly M (2020) Polymerization reactions and modifications of polymers by ionizing radiation. Polymer 12(12):2877
47. Shabbir M, Raza ZA, Shah TH, Tariq MR (2022) Recent progress in graphenes: synthesis, covalent functionalization and environmental applications. J Nanostructure Chem 12(6):1033–1051
48. Majumder M, Thakur AK (2019) Graphene and its modifications for supercapacitor applications. Surf Eng, pp 113–138
49. Lomeda JR, Doyle CD, Kosynkin DV, Hwang WF, Tour JM (2008) Diazonium functionalization of surfactant-wrapped chemically converted graphene sheets. J Am Chem Soc 130(48):16201–16206
50. Chua CK, Pumera M (2013) Covalent chemistry on graphene. Chem Soc Rev 42(8):3222–3233
51. Johns JE, Hersam MC (2013) Atomic covalent functionalization of graphene. Acc Chem Res 46(1):77–86
52. Sharma R, Baik JH, Perera CJ, Strano MS (2010) Anomalously large reactivity of single graphene layers and edges toward electron transfer chemistries. Nano Lett 10(2):398–405
53. Xu X, Chen J, Luo X, Lu J, Zhou H, Wu W, Li Z (2012) Poly (9, 9′-diheylfluorene carbazole) functionalized with reduced graphene oxide: convenient synthesis using nitrogen-based nucleophiles and potential applications in optical limiting. Chem Eur J 18(45):14384–14391
54. Li PP, Chen Y, Zhu J, Feng M, Zhuang X, Lin Y, Zhan H (2011) Charm-bracelet-type Poly (N-Vinylcarbazole) functionalized with reduced graphene oxide for broadband optical limiting. Chem Eur J 17(3):780–785
55. Wojtaszek M, Tombros N, Caretta A, Van Loosdrecht PHM, Van Wees BJ (2011) A road to hydrogenating graphene by a reactive ion etching plasma. J Appl Phys 110(6):063715
56. Medeiros PV, Mascarenhas AJ, de Brito MF, de Castilho CM (2010) A DFT study of halogen atoms adsorbed on graphene layers. Nanotechnology 21(48):485701
57. Robinson Jeremy T, James S, Chad Junkermeier E, Stefan Badescu C, Thomas L, Keith Perkins F, Maxim ZK (2010) Properties of fluorinated graphene films. Nano Lett 10(8):3001–3005
58. Chua CK, Pumera M (2012) Friedel-crafts acylation on graphene. Chem Asian J 7(5):1009–1012
59. Yuan C, Chen W, Yan L (2012) Amino-grafted graphene as a stable and metal-free solid basic catalyst. J Mater Chem 22(15):7456–7460
60. Zhan J, Lei Z, Zhang Y (2022) Non-covalent interactions of graphene surface: mechanisms and applications. Chem 8(4):947–979
61. Mao HY, Lu YH, Lin JD, Zhong S, Wee ATS, Chen W (2013) Manipulating the electronic and chemical properties of graphene via molecular functionalization. Prog Surf Sci 88(2):132–159
62. Guo X (2013) Single-molecule electrical biosensors based on single-walled carbon nanotubes. Adv Mater 25(25):3397–3408
63. Lin Y, Taylor S, Li H, Fernando KS, Qu L, Wang W, Sun YP (2004) Advances toward bioapplications of carbon nanotubes. J Mater Chem 14(4):527–541
64. Ma H, Shen Z (2020) Exfoliation of graphene nanosheets in aqueous media. Ceram Int 46(14):21873–21887
65. Brisebois PP, Siaj M (2020) Harvesting graphene oxide–years 1859 to 2019: a review of its structure, synthesis, properties and exfoliation. J Mater Chem C 8(5):1517–1547

66. Ghosh A, Rao KV, George SJ, Rao CNR (2010) Noncovalent functionalization, exfoliation, and solubilization of graphene in water by employing a fluorescent coronene carboxylate. Chem Eur J 16(9):2700–2704
67. Englert JM, Röhrl J, Schmidt CD, Graupner R, Hundhausen M, Hauke F, Hirsch A (2009) Soluble graphene: generation of aqueous graphene solutions aided by a perylenebisimide-based bolaamphiphile. Adv Mater 21(42):4265–4269
68. Bai H, Xu Y, Zhao L, Li C, Shi G (2009) Non-covalent functionalization of graphene sheets by sulfonated polyaniline. Chem Commun 13:1667–1669
69. Ibrahim A, Klopocinska A, Horvat K, Abdel Hamid Z (2021) Graphene-based nanocomposites: synthesis, mechanical properties, and characterizations. Polym 13(17):2869
70. Lawal AT (2020) Recent progress in graphene based polymer nanocomposites. Cogent Chem. 6(1):1833476
71. Zhou T, Zheng Y, Gao H, Min S, Li S, Liu HK, Guo Z (2015) Surface engineering and design strategy for surface-amorphized TiO_2@graphene hybrids for high power Li-ion battery electrodes. Adv Sci 2(9):1500027
72. Shi S, Chen F, Ehlerding EB, Cai W (2014) Surface engineering of graphene-based nanomaterials for biomedical applications. Bioconjug Chem 25(9):1609–1619
73. Azizi-Lalabadi M, Hashemi H, Feng J, Jafari SM (2020) Carbon nanomaterials against pathogens; the antimicrobial activity of carbon nanotubes, graphene/graphene oxide, fullerenes, and their nanocomposites. Adv Colloid Interface Sci 284:102250
74. Bhattacharya M (2016) Polymer nanocomposites—a comparison between carbon nanotubes, graphene, and clay as nanofillers. Mater 9(4):262
75. Nandee R, Chowdhury MA, Ahmed MU, Shuvho BA, Debnath UK (2019) Performance and characterization of two-dimensional material graphene conductivity-a review. Mater Perform Charact 8(1):183–196
76. Clancy AJ, Bayazit MK, Hodge SA, Skipper NT, Howard CA, Shaffer MS (2018) Charged carbon nanomaterials: redox chemistries of fullerenes, carbon nanotubes, and graphenes. Chem Rev 118(16):7363–7408
77. Cui Y, Kundalwal SI, Kumar S (2016) Gas barrier performance of graphene/polymer nanocomposites. Carbon 98:313–333
78. Zhao HY, Yu MY, Liu J, Li X, Min P, Yu ZZ (2022) Efficient preconstruction of three-dimensional graphene networks for thermally conductive polymer composites. Nano-Micro Lett 14(1):129
79. Zhu X, Ni Z, Dong L, Yang Z, Cheng L, Zhou X, Chen M (2019) In-situ modulation of interactions between polyaniline and graphene oxide films to develop waterborne epoxy anticorrosion coatings. Prog Org Coat 133:106–116
80. Zhu Q, Li EN, Liu X, Song W, Li Y, Wang X, Liu C (2020) Epoxy coating with in-situ synthesis of polypyrrole functionalized graphene oxide for enhanced anticorrosive performance. Prog Org Coat 140:105488
81. Zheng W, Lu X, Wong SC (2004) Electrical and mechanical properties of expanded graphite-reinforced high-density polyethylene. J Appl Polym Sci 91:2781–2788
82. Hu HT, Wang JC, Wan L, Liu FM, Zheng H (2010) Preparation and properties of graphene nanosheets—polystyrene nanocomposites via in-situ emulsion polymerization. Chem Phy Lett 484:247–253
83. Ye L, Meng XY, Ji X, Li ZM, Tang JH (2009) Synthesis and characterization of expandable graphite-poly(methyl methacrylate) composite particles and their application to flame retardation of rigid polyurethane foams. Polym Degrad Stab 94:971–979
84. Chen G, Wu D, Weng W, Wu C (2003) Exfoliation of graphite flakes and its nanocomposites. Carbon 41:619–621
85. Kornmann X (2001) Synthesis and characterization of thermoset-layered silicate nanocomposites. Ph.D. thesis. Sweden, Lulea Tekniska Universitet
86. Moujahid EM, Besse JP, Leroux F (2003) Poly(styrene sulfonate) layered double hydroxide nanocomposites Stability and subsequent structural transformation with changes in temperature. J Mater Chem 13:258–264

87. Hsueh HB, Chen CY (2003) Preparation and properties of LDHs= polyimide nanocomposites. Polym 44:1151–1161
88. Novoselov KS, Geim AK, Morozov SV (2004) Electric field effect in atomically thin carbon films. Science 306:666–669
89. Tkalya E, Ghislandi M, Alekseev A (2010) Latex-based concept for the preparation of graphene-based polymer nanocomposites. J Mater Chem 20:3035–3039
90. Latif I, Alwan TB, Al-Dujaili AH (2012) Low frequency dielectric study of PAPA-PVA-GR nanocomposites. Nanosci Nanotechnol 2:190–200
91. Murugan AV, Muraliganth T, Manthiram A (2009) Rapid, facile microwave-solvothermal synthesis of graphene nanosheets and their polyaniline nanocomposites for energy strorage. Chem Mater 21:5004–5006
92. Fan X, Peng W, Li Y (2008) Deoxygenation of exfoliated graphite oxide under alkaline conditions: a green route to graphene preparation. Adv Mater 2:4490–4493
93. Park S, An J, Jung I (2009) Colloidal suspensions of highly reduced graphene oxide in a wide variety of organic solvents. Nano Lett 9:1593–1597
94. Jiang L, Shen XP, Wu JL (2010) Preparation and characterization of graphene/poly (vinyl alcohol) nanocomposites. J Appl Polym Sci 118:275–279
95. Bourlinos AB, Gournis D, Petridis D (2003) Graphite oxide: chemical reduction to graphite and surface modification with primary aliphatic amines and amino acids. Langmuir 19:6050–6055
96. Wang G, Shen X, Yao J (2009) Graphene nanosheets for enhanced lithium storage in lithium ion batteries. Carbon 47:2049–2053
97. Staudenmaier L (1898) Verfahren zur darstellung der graphitsa¨ure. Ber Dtsch Chem Ges 31:1481–1499
98. Michael J, McAllister J-L (2007) Single sheet functionalized graphene by oxidation and thermal expansion of graphite. Chem Mater 19:4396–4404
99. Zhang HB, Zheng WG, Yan Q (2010) Electrically conductive polyethylene terephthalate/graphene nanocomposites prepared by melt compounding. Polym 51:1191–1196
100. Potts JR, Dreyer DR, Bielawski CW (2011) Graphene based polymer nanocomposites. Polymer 52:5–25
101. Hu H, Wang X, Wang J (2010) Preparation and properties of graphene nanosheets–polystyrene nanocomposites via in situ emulsion polymerization. Chem Phys Lett 484:247–253
102. Patole AS, Patole SP, Kang H (2010) A facile approach to the fabrication of graphene/polystyrene nanocomposite by in situ microemulsion polymerization. J Colloid Interface Sci 350:530–537
103. Ni Z, Wang Y, Yu T (2008) Raman spectroscopy and imaging of graphene. Nano Res 1:273–291
104. Gawryla MD, van den Berg O, Weder C (2009) Clay aerogel/cellulose whisker nanocomposites: a nanoscale wattle and daub. J Mater Chem 19:2118–2124
105. Van den Berg O, Capadona JR, Weder C (2007) Preparation of homogeneous dispersions of tunicate cellulose whiskers in organic solvents. Biomacromol 8:1353–1357
106. Chen W, Yan L, Bangal PR (2010) Preparation of graphene by the rapid and mild thermal reduction of graphene oxide induced by microwaves. Carbon 48:1146–1152
107. Chen W, Yan L (2010) Preparation of graphene by a low temperature thermal reduction at atmosphere pressure. Nanoscale 2:559–563
108. Zhou X, Liu Z (2010) A scalable, solution-phase processing route to graphene oxide and graphene ultra large sheets. Chem Commun 46:2611–2613
109. Vickery JL, Patil AJ, Mann S (2009) Fabrication of graphene–polymer nanocomposites with higher-order three dimensional architectures. Adv Mater 21:2180–2184
110. Cao Y, Feng J, Wu P (2010) Preparation of organically dispersible graphene nanosheet powders through a lyophilization method and their poly (lactic acid) composites. Carbon 48:3834–3839
111. Chaturvedi A, Tiwari A, Tiwari A (2013) Spectroscopic and morphological analysis of graphene vinylester nanocomposites. Adv Mater Lett 4:656–661

112. Che J, Shen L, Xiao Y (2010) A new approach to fabricate graphene nanosheets in organic medium: combination of reduction and dispersion. J Mater Chem 20:1722–1727
113. Gong L, Kinloch IA, Young RJ (2010) Interfacial stress transfer in a graphene monolayer nanocomposite. Adv Mater 22:2694–2697
114. Liu P, Huang Y, Wang L (2013) Preparation and excellent microwave absorption property of three component nanocomposites: Polyaniline-reduced graphene oxide-CO_3O_4 nanoparticles. Synth Met 177:89–93
115. Marcano DC, Kosynkin DV, Berlin JM (2010) Improved synthesis of graphene oxide. ACS Nano 4:4806–4814
116. Kumar SK, Castro M, Saiter A (2013) Development of poly (isobutylene-coisoprene)/reduced graphene oxide nanocomposites for barrier, dielectric and sensing applications. Mater Lett 96:109–112
117. Zeng X, Yang J, Yuan W (2012) Preparation of a poly (methyl methacrylate)-reduced graphene oxide composite with enhanced properties by a solution blending method. Eur Polym J 48:1674–1682
118. Subrahmanyam K, Vivekchand S, Govindaraj A (2008) A study of graphenes prepared by different methods: characterization, properties and solubilization. J Mater Chem 18:1517–1523
119. Zaman I, Kuan HC, Dai J (2012) From carbon nanotubes and silicate layers to graphene platelets for polymer nanocomposites. Nanoscale 4: 4578–4586
120. Yu J, Lu K, Sourty E, Grossiord N, Koning CE, Loos J (2007) Characterization of conductive multiwall carbon nanotube/polystyrene composites prepared by latex technology. Carbon 45:2897–2903
121. Li J, Vaisman L, Marom G, Kim JK (2007) Br treated graphite nanoplatelets for improved electrical conductivity of polymer composites. Carbon 45:744–750
122. Wang S, Tambraparni M, Qiu J, Tipton J, Dean D (2009) Thermal expansion of graphene composites. Macromolecules 42:5251–5255
123. Kuilla T, Srivastava SK, Bhowmick AK (2009) Rubber/LDH nanocomposites by solution blending. J Appl Polym Sci 111:635–641
124. Yu A, Ramesh P, Itkis ME, Elena B, Haddon RC (2007) Graphite nanoplatelet-epoxy composite thermal interface materials. J Phys Chem C 111:7565–7569
125. Liu N, Luo F, Wu H, Liu Y, Zhang C, Chen J (2008) One step ionic-liquid assisted electrochemical synthesis of ionic-liquid-functionalized graphene sheets directly from graphene. Adv Funct Mater 18:1518–1525
126. Eda G, Chhowalla M (2009) Graphene-based composite thin films for electronics. Nano Lett 9:814–818
127. Mu Q, Feng S (2007) Thermal conductivity of graphite/silicone rubber prepared by solution intercalation. Thermochim Acta 462:70–75
128. Zhang HB, Zheng WG, Yan Q, Yang Y, Wang J, Lu ZH (2010) Electrically conductive polyethylene terephthalate/graphene nanocomposites prepared by melt compounding. Polymer 51:1191–1196
129. Hu H, Wang X, Wanga J, Wana L, Liu F, Zheng H (2010) Preparation and properties of graphene nanosheets-polystyrene nanocomposites via in situ emulsion polymerization. Chem Phys Lett 484:247–253
130. Stankovich S, Dikin DA, Piner RD, Kohlhaas KA, Kleinhammes A (2007) Synthesis of graphene-based nanosheets via chemical reduction of exfoliated graphite oxide. Carbon 45:1558–1565
131. Zhao X, Zhang Q, Chen D (2010) Enhanced mechanical properties of graphene-based poly(vinyl alcohol) composites. Macromolecules 43:2357–2363
132. Stankovich S, Dikin DA, Dommett GHB, Kohlhaas KM, Zimney EJ, Stach EA (2006) Graphene-based composite materials. Nature 442:282–286
133. Liu N, Luo F, Wu H, Liu Y, Zhang C, Chen J (2008) One step ionicliquidassisted electrochemical synthesis of ionic-liquid-functionalized graphene sheets directly from graphene. Adv Funct Mater 18:1518–1525

134. Mu Q, Feng S (2007) Thermal conductivity of graphite=silicone rubber prepared by solution intercalation. Thermochim Acta 462:70–75
135. Hu HT, Wang JC, Wan L, Liu FM, Zheng H (2010) Preparation and properties of graphene nanosheets—polystyrene nanocomposites via insitu emulsion polymerization. Chem Phys Lett 484:247–253
136. Kuilla T, Bhadra S, Yao D, Kim NH, Bose S, Lee JH (2010) Recent advances in graphene based polymer composites. Prog Poly Sci 35(11):1350–1375
137. Peponi L, Tercjak A, Verdejo R, Lopez-Manchado MA, Mondragon I, Kenny JM (2009) Confinement of functionalized graphene sheets by triblock copolymers. J Phys Chem 113:17973–17978
138. Wang DW, Li F, Zhao J, Ren W, Chen ZG, Tan J (2009) Fabrication of graphene/polyaniline composite paper via in situ anodic electro-polymerization for high-performance flexible electrode. ACS Nano 7:1745–1752
139. Zhao L, Zhao L, Xu Y, Qiu T, Zhi L, Shi G (2009) Polyaniline electrochromic devices with transparent graphene electrodes. Electrochim Acta 55:491–497
140. Yan J, Wei T, Fan Z, Qian W, Zhang M, Shen X (2010) Preparation of graphene nanosheet/carbon nanotube/polyaniline composite as electrode material for supercapacitors. J Power Sources 195:3041–3045
141. Mazinani S, Ajji A, Dubois C (2009) Morphology, structure and properties of conductive PS=CNT nanocomposite electrospun mat. Polym 50:3329–3342
142. Bourlinos AB, Gournis D, Petridis D, Szabo T, Szeri A, Dekany I (2003) Graphite oxide: chemical reduction to graphite and surface modification with primary aliphatic amines and amino acids. Chem Mater 19:6050–6055
143. Liang J, Huang Y, Zhang L, Wang Y, Ma Y, Guo T (2009) Molecular-level dispersion of graphene into poly(vinyl alcohol) and effective reinforcement of their nanocomposites. Adv Funct Mater 19:2297–2302
144. Lee YR, Raghu AV, Jeong HM, Kim BK (2009) Properties of waterborne polyurethane/functionalized graphene sheet nanocomposites prepared by an in situ method. Macromol Chem Phys 210(15):1247–1254
145. Liang J, Xu Y, Huang Y, Zhang L, Wang Y, Ma Y (2009) Infraredtriggered actuators from graphene-based nanocomposites. J Phys Chem 113:9921–9927
146. Ansari S, Giannelis EP (2009) Functionalized graphene sheetpoly(vinylidene fluoride) conductive nanocomposites. J Polym Sci Part B Polym Phys 47:888–897
147. Xu Y, Wang Y, Jiajie L, Huang Y, Ma Y, Wan X (2009) A hybrid material of graphene and poly(3,4-ethyldioxythiophene) with high conductivity, flexibility, and transparency. Nano Res 2:343–348
148. Kim H, Macosko CW (2009) Processing–property relationships of polycarbonate/graphene nanocomposites. Polym 50:3797–3809
149. Cussler EL, Hughes SE, Ward WJ III, Aris R (1988) Barrier membrane. J Membr Sci 38:161–174
150. Halperin BI, Feng S, Sen PN (1985) Differences between lattice and continuum percolation transport exponents. Phys Rev Lett 54:2391–2394
151. Moussa M, El-Kady MF, Zhao Z, Majewski P, Ma J (2016) Recent progress and performance evaluation for polyaniline/graphene nanocomposites as supercapacitor electrodes. Nanotechnology (27):442001
152. Tai Z, Yan X, Xue Q (2012) Three-dimensional graphene/polyaniline composite hydrogel as supercapacitor electrode. J Electrochem Soc 159(10):A1702
153. Liu H, Wang Y, Gou X, Qi T, Yang J, Ding Y (2013) Three-dimensional graphene/polyaniline composite material for high-performance supercapacitor applications. Mater Sci Eng 5:293–298
154. Kulkarni SB, Patil UM, Shackery I, Sohn JS, Lee S, Park B, Jun S (2014) High-performance supercapacitor electrode based on a polyaniline nanofibers/3D graphene framework as an efficient charge transporter. J Mater Chem A 14:4989–4998

155. Zhang Y, Huang Y, Yang G, Bu F, Li K, Shakir I, Xu Y (2017) Dispersion–assembly approach to synthesize three-dimensional graphene/polymer composite aerogel as a powerful organic cathode for rechargeable Li and Na batteries. ACS Appl Mater Interf 18:15549–15556
156. Li WW, Yu HQ, He Z (2014) Towards sustainable wastewater treatment by using microbial fuel cells-centered technologies. Energy Environ Sci 3:911–924
157. Xie X, Criddle C, Cui Y (2015) Design and fabrication of bioelectrodes for microbial bioelectrochemical systems. Energy Environ Sci 12:3418–3441
158. Zou L, Qiao Y, Wu ZY, Wu XS, Xie JL, Yu SH, Li CM (2016) Tailoring unique mesopores of hierarchically porous structures for fast direct electrochemistry in microbial fuel cells. Adv Energy Mater 4:1501535
159. Yang Y, Dong R, Zhu Y, Li H, Zhang H, Fan X, Chang H (2020) High-performance direct hydrogen peroxide fuel cells (DHPFCs) with silver nanowire-graphene hybrid aerogel as highly-conductive mesoporous electrodes. Chem Eng J 381:122749
160. Du Q, An J, Li J, Zhou L, Li N, Wang X (2017) Polydopamine as a new modification material to accelerate startup and promote anode performance in microbial fuel cells. J Power Sources 343:477–482
161. Tang C, Zhang Q (2016) Can metal–nitrogen–carbon catalysts satisfy oxygen electrochemistry? J Mater Chem A 14:4998–5001
162. Yong YC, Dong XC, Chan-Park MB, Song H, Chen P (2012) Macroporous and monolithic anode based on polyaniline hybridized three-dimensional graphene for high-performance microbial fuel cells. ACS Nano 6(3):2394–2400
163. Xia H, Hong C, Li B, Zhao B, Lin Z, Zheng M, Aldoshin SM (2015) Facile synthesis of hematite quantum-dot/functionalized graphene-sheet composites as advanced anode materials for asymmetric supercapacitors. Adv Funct Mater 25(4):627–635